Gondwana Research 19 (2011) 735–750

Contents lists available at ScienceDirect

Gondwana Research

journal homepage: www.elsevier.com/locate/gr

The Rio Capim volcanic–plutonic–sedimentary belt, São Francisco Craton, Brazil: Geological, geochemical and isotopic evidence for oceanic arc accretion during Palaeoproterozoic continental collision

E.P. Oliveira [a,*], Z.S. Souza [b], N.J. McNaughton [c], J.-M. Lafon [d], F.G. Costa [a], A.M. Figueiredo [e]

[a] Department of Geology and Natural Resources, Geosciences Institute, University of Campinas, P.O. Box 6152, Campinas, SP, 13083-970, Brazil
[b] Departamento de Geologia e Pós-Graduação em Geodinâmica e Geofísica, UFRN, Natal, RN, 59078-970, Brazil
[c] John de Laeter Centre of Mass Spectrometry, School of Applied Physics, Curtin University of Technology, Perth, WA 6845, Australia
[d] Instituto de Geociências, Universidade Federal do Pará, Belém, PA, 66075-110, Brazil
[e] Instituto de Pesquisas Energéticas e Nucleares — IPEN-CNEN/SP, São Paulo, SP, 05508-000, Brazil

ARTICLE INFO

Article history:
Received 14 January 2010
Received in revised form 9 June 2010
Accepted 16 June 2010
Available online 1 July 2010

Keywords:
Arc–continent collisions
Precambrian oceanic arcs
São Francisco craton
Palaeoproterozoic plate tectonics

ABSTRACT

The collision of oceanic arcs with continents is a common plate tectonic process in the Phanerozoic, but its recognition in the Precambrian is hampered by deformation and metamorphism. The Rio Capim volcanic–plutonic–sedimentary belt lies in sharp tectonic contact with Archaean rocks of the Uauá block in the northern part of the São Francisco craton. Field relationships and high-precision geochronology indicated that the Rio Capim basalts, gabbros, diorites, and dacites were emplaced approximately at 2148–2143 Ma, and later intruded by 2128 Ma-old diorite to tonalite plutons. All rocks were metamorphosed under amphibolite to granulite facies conditions mainly between 2080 Ma and 2070 Ma, but deformation may have lasted until about 2040 Ma as estimated from syn-deformation zircon and titanite grains. The association of basalt, andesite, dacite, and their plutonic counterparts, combined with their positive $\varepsilon_{Nd}(t)$ values and incompatible trace element geochemical signatures similar to island arc magmas, support the proposition that the Rio Capim belt was a Palaeoproteorozoic intra-oceanic arc sequence that collided with a continent, of which the Mesoarchaean Uauá block is a remnant. The implications for the regional evolution and metallogenesis are also discussed.

1. Introduction

In present-day Earth arc magmatism in both oceanic and continental tectonic settings is generally invoked as one of the two major sources of mantle-derived (juvenile) material to make the continents grow; the other is input from mantle plumes (e.g., Safonova et al., 2009; Isozkai et al., 2010). However, the recognition of ancient arc assemblages in the geological record is not simple because of the processes that occur along the boundaries of tectonic plates. For instance, when an intra-oceanic arc collides with a continental margin, both the arc rocks and the continent may undergo deformation, high-grade metamorphism, and be intruded by syn- to post-collision granite plutons. This geological scenario may be further complicated if the rock assemblages, or terranes are displaced laterally by strike-slip tectonics. One Phanerozoic example is the accreted Kohistan island arc in the western Himalaya orogen which was intruded by the Andean-style Kangdese batholith before final collision between India and Asia, and extrusion tectonics (Bignold and Treloar, 2003).

Brazil has no active arc or collisional orogen, but the country is underlain by a wealth of Precambrian orogenic belts and cratons. This makes the Precambrian of Brazil a suitable place to look for ancient accretionary orogens with continental and oceanic arcs. For example, the Amazon craton has now been interpreted as having grown by lateral accretion of arcs with ages varying from 2.3 Ga to 1.0 Ga (Tassinari and Macambira, 1999; Ruiz et al., 2004; Santos et al., 2004; Cordani and Teixeira, 2007; Cordani et al., 2009; Teixeira et al., 2010), and in the São Francisco craton several arc batholiths and accretionary orogens were recognized (e.g. Barbosa, 1990; Teixeira and Figueiredo, 1991; Delgado et al., 2003; Ávila et al., 2006; Oliveira et al., 2010).

Here, we present new geological, geochemical and isotopic data for the Rio Capim belt, which is a sequence of plutonic-supracrustal high-grade rocks exposed in the Serrinha block (microcontinent) of the São Francisco craton. The belt is composed of Palaeoproterozoic fine- and coarse-grained mafic igneous rocks, metadacites, metapelites and several granite plutons, which are in tectonic contact with the Archaean Uauá block. Our results support the interpretation that the Rio Capim belt was part of a dismembered oceanic arc that collided with a continental plate, and provide direct evidence of plate

* Corresponding author. Fax: +55 19 32891562.
E-mail address: elson@ige.unicamp.br (E.P. Oliveira).

1342-937X/$ – see front matter
doi:10.1016/j.gr.2010.06.005

tectonics processes, as we know in the Phanerozoic, as far back as the early Palaeoproterozoic.

2. Regional geology

The main geologic features of the São Francisco craton are outlined in Teixeira and Figueiredo (1991) and Teixeira et al. (2000). In general, the São Francisco Craton consists of Archaean to Palaeoproterozoic high-grade (migmatite, granulite) gneisses and granite–greenstone supracrustal terranes overlain by Meso- to Neoproterozoic platform-type cover (Fig. 1). Typical greenstone belts with spinifex-textured komatiites occur in the iron quadrangle of Minas Gerais in the southernmost part of the craton (e.g. Lobato et al., 2001), and in the Umburanas region in the north (Cunha and Fróes, 1994). In the northern part of the São Francisco Craton greenstone belts such as the Rio Itapicuru, Mundo Novo, Rio Capim and Contendas–Mirante (Mascarenhas, 1979; Mascarenhas and Sá, 1982; Jardim de Sá et al., 1984; Davison et al., 1988; Peucat et al., 2002) contain no komatiites, and geochronological data have demonstrated that they range in age from ca. 3.3 Ga (Mundo Novo greenstone belt, Peucat et al., 2002) to ca. 2.1 Ga (e.g. Rio Itapicuru, Silva et al., 2001).

The high-grade terranes, mostly exposed in Bahia (Fig. 1), are traditionally separated into the Neoarchaean Jequié migmatite–granulite complex (Alibert and Barbosa, 1992; Barbosa and Sabaté, 2004), the Mesoarchaean to Palaeoproterozoic Serrinha block (Mascarenhas, 1979; Mello et al., 2006; Rios et al., 2009; Oliveira et al., 2010), and the Palaeoproterozoic-reworked Neoarchaean Itabuna–Salvador–Curaçá belt (Barbosa and Sabaté, 2004; Oliveira et al., 2010). The latter comprises a northern segment known as the Salvador–Curaçá belt (1 in Fig. 1) and a southern segment named the Atlantic coast granulite belt or Itabuna complex (2 in Fig. 1). The two segments are currently known as the Itabuna–Salvador–Curaçá orogen (Barbosa et al., 2001; Delgado et al., 2003; Oliveira et al., 2004a; Barbosa et al., 2008), as shown in Fig. 1.

All tectonic models proposed for the Itabuna–Salvador–Curaçá orogen during the Palaeoproterozoic involve a final stage of continent–continent collision similar to Phanerozoic orogens (Figueiredo, 1989; Barbosa, 1990; Teixeira and Figueiredo, 1991; Ledru et al., 1997; Teixeira et al., 2000; Silva et al., 2001; Oliveira et al., 2002; Barbosa and Sabaté, 2004; Oliveira et al., 2004a, 2010).

According to Barbosa and Sabaté (2004) the southern segment of the orogen is the final result of collision between the Gabon massif, in West Africa, and the Jequié microcontinent, in the following sequence:

1. (2.6–2.4 Ga) — accretion of a continental arc,
2. (2.4–2.2 Ga) — intrusion of shoshonitic to alkaline monzonite and monzodiorite plutons,
3. (2.07–2.08 Ga) — continent–continent collision and granulite facies metamorphism.

For the orogen's northern segment the geochronological and geological data point to a long cycle of basement reworking (Sabaté et al., 1994; Silva et al., 1997; Oliveira et al., 2000, 2004a,b; Silva et al., 2007), accretion of continental and oceanic arcs, and plutonic complexes to Archaean blocks (Teixeira and Figueiredo, 1991; Ledru et al., 1997; Silva et al., 2001; Delgado et al., 2003; Oliveira et al., 2004a,b, 2010). Final continental collision occurred between 2080 Ma and 2039 Ma, i.e. the age interval for the peak of high-grade metamorphism (Silva et al., 1997; Oliveira et al., 2002, 2004a; Mello et al., 2006; Leite et al., 2009; Oliveira et al., 2010).

Barbosa and Sabaté (2004) proposed that four Archaean tectonic blocks, namely Gavião, Serrinha, Jequié and the Itabuna–Salvador–Curaçá orogen have collided during the Palaeoproterozoic orogeny.

Because the Rio Capim belt lies within the Serrinha block, geological information on this block is relevant.

2.1. Serrinha block

The Serrinha block, or microcontinent (Fig. 2) comprises a basement complex of migmatites, banded gneisses, orthogneisses,

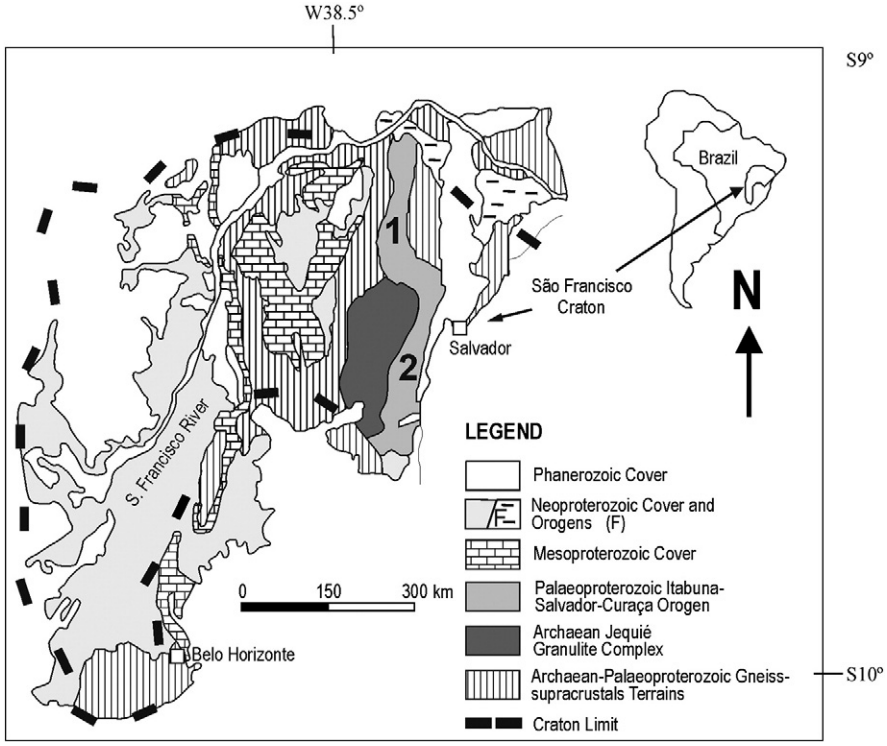

Fig. 1. The São Francisco Craton with the main tectonic units and location of the northern (1) and southern (2) segments of the Itabuna–Salvador–Curaçá orogen.

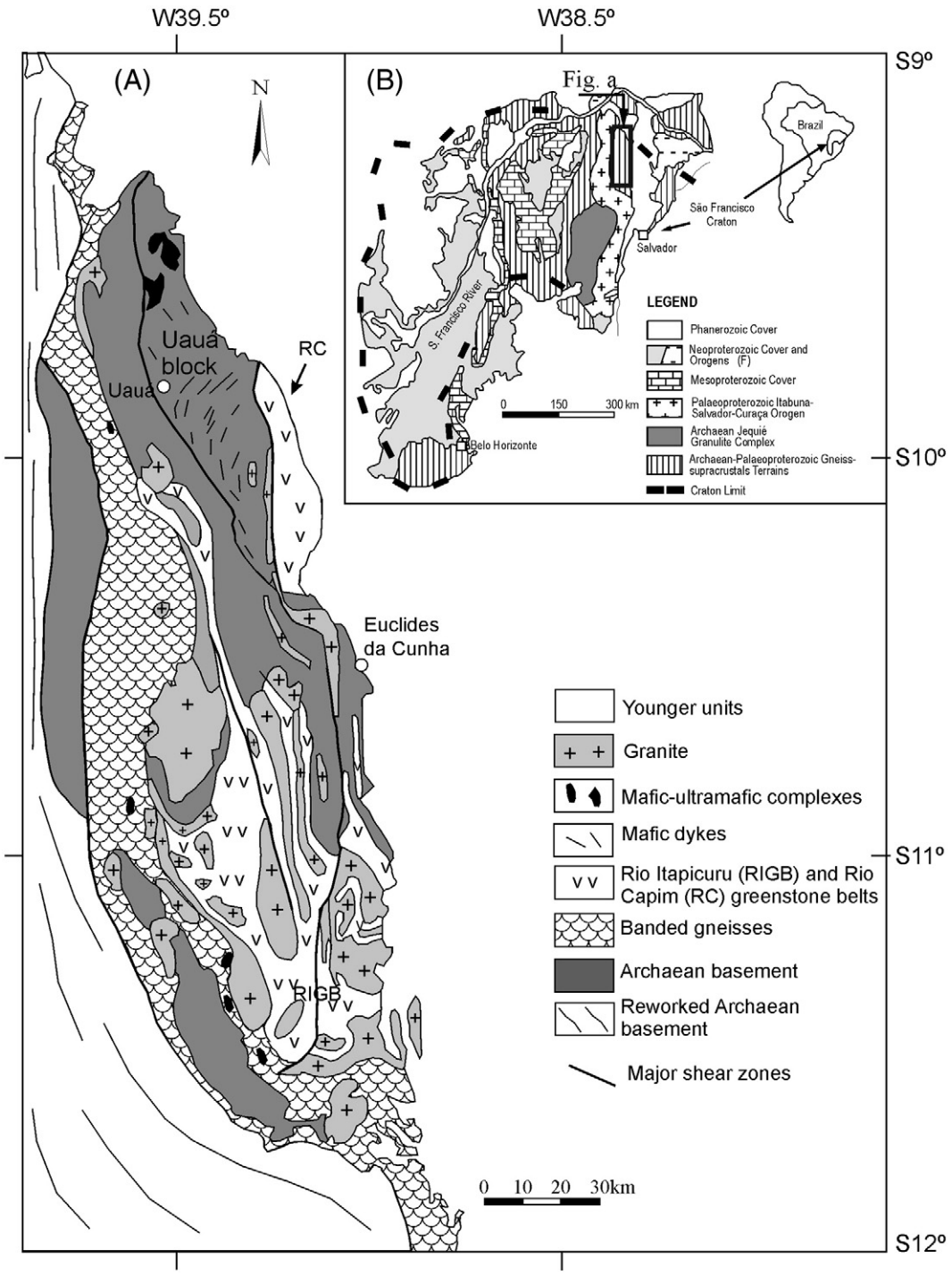

Fig. 2. Geological map of the Serrinha block with location of the Rio Capim belt (RC), Rio Itapicuru belt (RIGB) and the Uauá block (modified after CPRM-unpublished). Inset indicates location of the Serrinha block in the São Francisco craton.

mafic dykes and mafic–ultramafic complexes. This basement is overlain by, or lies in tectonic contact with supracrustal sequences of the Rio Itapicuru and Rio Capim belts, and of the Caldeirão shear belt. Granites intrude all units. The Uauá, Jacurici and Retirolândia gneiss–migmatite complexes (Fig. 2) are Mesoarchaean domains (3152–2933 Ma, Oliveira et al., 2004a, 2010), or minor blocks in the Serrinha block.

The Rio Itapicuru greenstone belt (RIGB in Fig. 2) is a low grade metamorphic supracrustal sequence 180 km long and 30 km wide, divided by Kishida and Riccio (1980) into three lithostratigraphic units: (i) the basal mafic volcanic unit composed of massive and pillowed basaltic flows interlayered with chert, banded iron-formation, and carbonaceous shale; (ii) the intermediate to felsic volcanic unit with metadacites, metandesites and metapyroclastic rocks, and (iii) a metasedimentary pelitic–psammitic unit composed mainly of metapelites and minor chemical sedimentary rocks. The geochronological data indicate a Palaeoproterozoic evolution for this belt, between 2170 Ma and 2080 Ma (Silva et al., 2001; Mello et al., 2006; Rios et al., 2009; Oliveira et al., 2010).

The Rio Capim belt (RC in Fig. 2) lies in contact with the Uauá block and for this reason the two tectonic units will be described in detail in the next sections.

2.2. The Uauá block

The Uauá block (Fig. 2) is bordered to the west by the Archaean–Palaeoproterozoic Caldeirão belt, and to the east it is unconformably overlain by Neoproterozoic continental shelf metasedimentary rocks of the Sergipano orogen (Bueno et al., 2009), or younger rock units.

The Caldeirão belt comprises a 10 km-thick sequence of steeply dipping quartzites, metapelites, orthogneisses, mafic rocks and migmatites; all metamorphosed under amphibolite facies conditions. The transition from this belt to the Uauá block is gradational and marked by refolding of older structures in the latter, granite and pegmatite intrusions, and development of shear zones, sometimes a few kilometres in width. Syn-deformational titanite in mafic dyke (Oliveira et al., 2000) and detrital zircon grains in quartzite (Oliveira et al., 2002) constrain a maximum deposition age of 2700 Ma and a metamorphic age between 2039 and 2077 Ma for the metasedimentary rocks.

The Uauá block consists mostly of NW-trending banded gneisses of unknown age intruded by layered anorthosite, peridotite and diorite complexes, and tonalite–granodiorite bodies (Mascarenhas and Sá, 1982; Cordani et al., 1999; Oliveira et al., 1999, 2010). Most of these rock units have been metamorphosed under granulite facies conditions and later retrogressed to amphibolite grade. Mesoarchaean rocks are widespread in the Uauá block. Paixão and Oliveira (1998) obtained a 3161 ± 65 Ma whole-rock Pb–Pb isochron for anorthosites of the Lagoa da Vaca layered anorthosite complex and zircon Pb-evaporation age of 3072 ± 20 Ma for orthogranulites, while Cordani et al. (1999) presented zircon U–Pb SHRIMP ages between 3.12 and 3.13 Ga for the Capim tonalite. Several other Archaean felsic igneous bodies occur in the Uauá block, some of which, i.e. the Uauá quarry enderbitic granulite and a gneissic granodiorite to the southeast of Uauá were respectively dated at 2933 ± 3 Ma and 2991 ± 22 Ma (Oliveira et al., 2002); the latter entrain xenoliths of the country-rock banded gneisses. Two mafic dyke swarms intrude the basement; an old NW–SE-trending swarm made up of amphibolite dykes and a young NE–SW-trending swarm made up of tholeiite and norite dykes. Samples from the young dykes yielded a reference Sm–Nd isochron of 2586 ± 66 Ma (Oliveira et al., 1999). The latter dykes change their NE–SW direction to NW–SE as they approach the Caldeirão shear belt, where the dykes have been boudined, disrupted and metamorphosed to amphibolites. The observed dyke curvature is related to northward displacement of the Uauá block during oblique continent–continent collision between 2039 and 2077 Ma (Oliveira et al., 2002, 2010).

3. The Rio Capim belt

This belt (Fig. 3) is a relatively small, 4-km wide on its southern and northern tips, and about 10-km wide on the larger central region, 20-km long, N-, to NW-trending belt of deformed and metamorphosed mafic to felsic volcanic rocks and associated sedimentary rocks, intruded by several plutons ranging in composition from gabbro-diorite to granite. The Rio Capim belt lies in contact with Archaean rocks of the Uauá block, to the west,

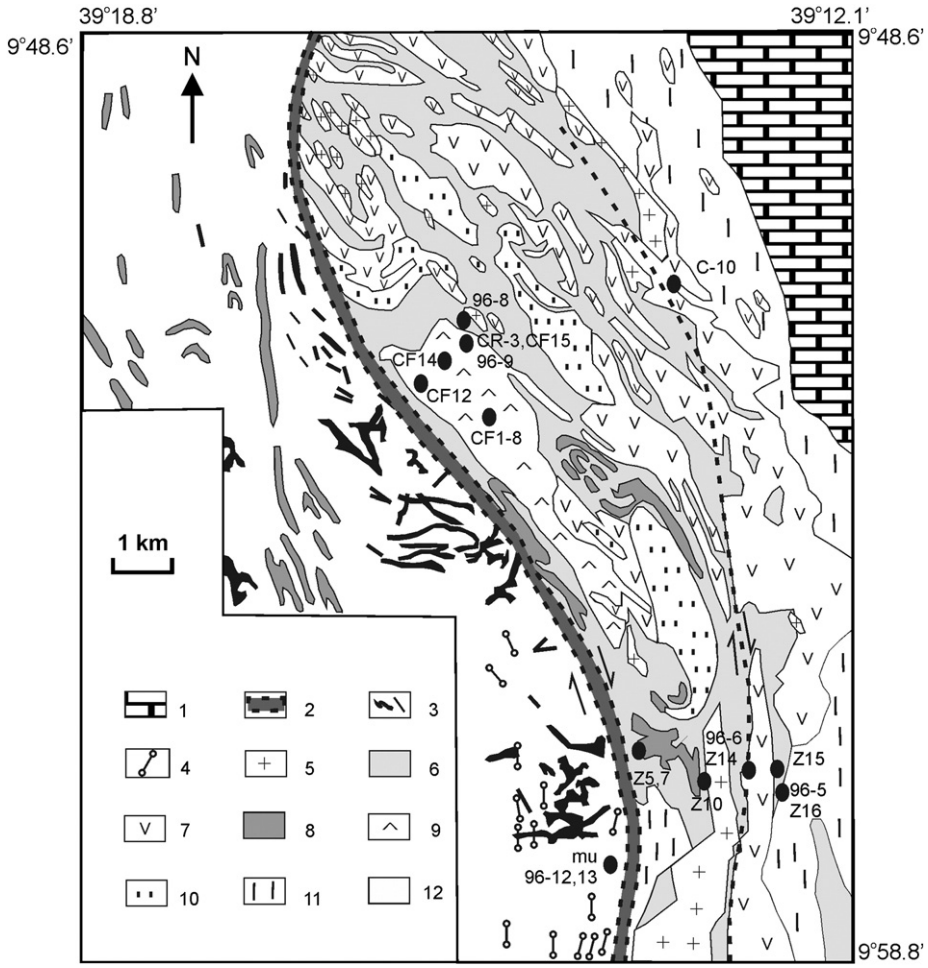

Fig. 3. Geological map of the Rio Capim belt with sample location (modified after Jardim de Sá et al., 1984). 1 — Nappes of Sergipano belt Neoproterozoic sedimentary rocks; 2 — Shear zone, grey ornamented — Galo do Ouro shear zone; 3 — Mafic dyke and irregular bodies; 4 to 11 — Rio Capim belt: 4 — Felsic dyke; 5 — Granitic orthogneisses and pegmatites; 6 — Felsic and mafic metavolcanics, and intercalated metasedimentary rocks; 7 — Metagabbro/medium- to coarse grained amphibolite; 8 — Fine grained amphibolite; 9 — Felsic lava and tuffs; 10 — Amphibolite and intercalated metasedimentary rocks; 11 — Tonalitic to quartz–dioritic orthogneisses; 12 — Archaean basement.

by the sub-vertical sigmoidal S-shaped kilometre scale Galo do Ouro shear zone (Figs. 3 and 4A); to the east it is overlain by Neoproterozoic sedimentary rocks of the Sergipano belt. The Rio Capim belt is metallogenetically interesting for its massive sulfide occurrences (pyrite and pyrrhotite).

Mapping the Rio Capim belt is not an easy task, owing to its lithological diversity and structural complexity. Winge and Danni (1980), Jardim de Sá et al. (1984), Souza (1984) and Fonseca (1986) recognized the following main rock associations:

- metabasalts (Fig. 4B) and mafic to felsic metatuffs interleaved with pelitic (Fig. 4C) metasedimentary rocks (garnet–biotite–sillimanite–cordierite schist, graphite schist, biotite gneiss) and chemical to volcanic–chemical metasedimentary rocks (banded iron formation, ferrugineous and carbonatic cherts);
- metadacites (Fig. 4d) to meta-quartz andesites, locally porphyritic;
- gabbroic and granitic intrusions (Fig. 4e,f);
- felsic dykes to the SW intrusive into the Uauá block and texturally comparable with the felsic volcanic rocks within the central portion of the Rio Capim belt.

The relationships between mafic and felsic metavolcanic rocks is unclear. However, because the felsic metavolcanics crop out mostly in the central part of the Rio Capim belt, within a large scale, gently open antiform, have decimetre- to metric scale metabasalt enclaves, and appear as narrow sills in metasedimentary rocks, Winge (1981), Jardim de Sá et al. (1984), and Souza (1984) suggested that felsic metavolcanics might be younger than the metasedimentary and metabasaltic rocks.

A detailed description of the structural and metamorphic evolution of the Rio Capim Belt is presented in Jardim de Sá et al. (1984) and Souza (1984, 1986), hence only a summary is given here. Accordingly, the main foliation of the Rio Capim rocks is a composite fabric of $S_1 + S_2$, which can be clearly seen on F_2 fold hinges. S_1 is a low angle foliation that broadly parallels the original igneous and sedimentary structures (S_0), or the axial plane of intrafolial folds, and both structures are folded and boudined by F_2.

Metamorphism (M_2) accompanying deformation F_2 is of the low-pressure type and shows remarkable variation across the Rio Capim belt. Thus, from west to east M_2 gradually increases from low amphibolite to low pressure–high temperature granulite facies. The mafic rocks consist mostly of hornblende + plagioclase (An28–32) in the west, grading

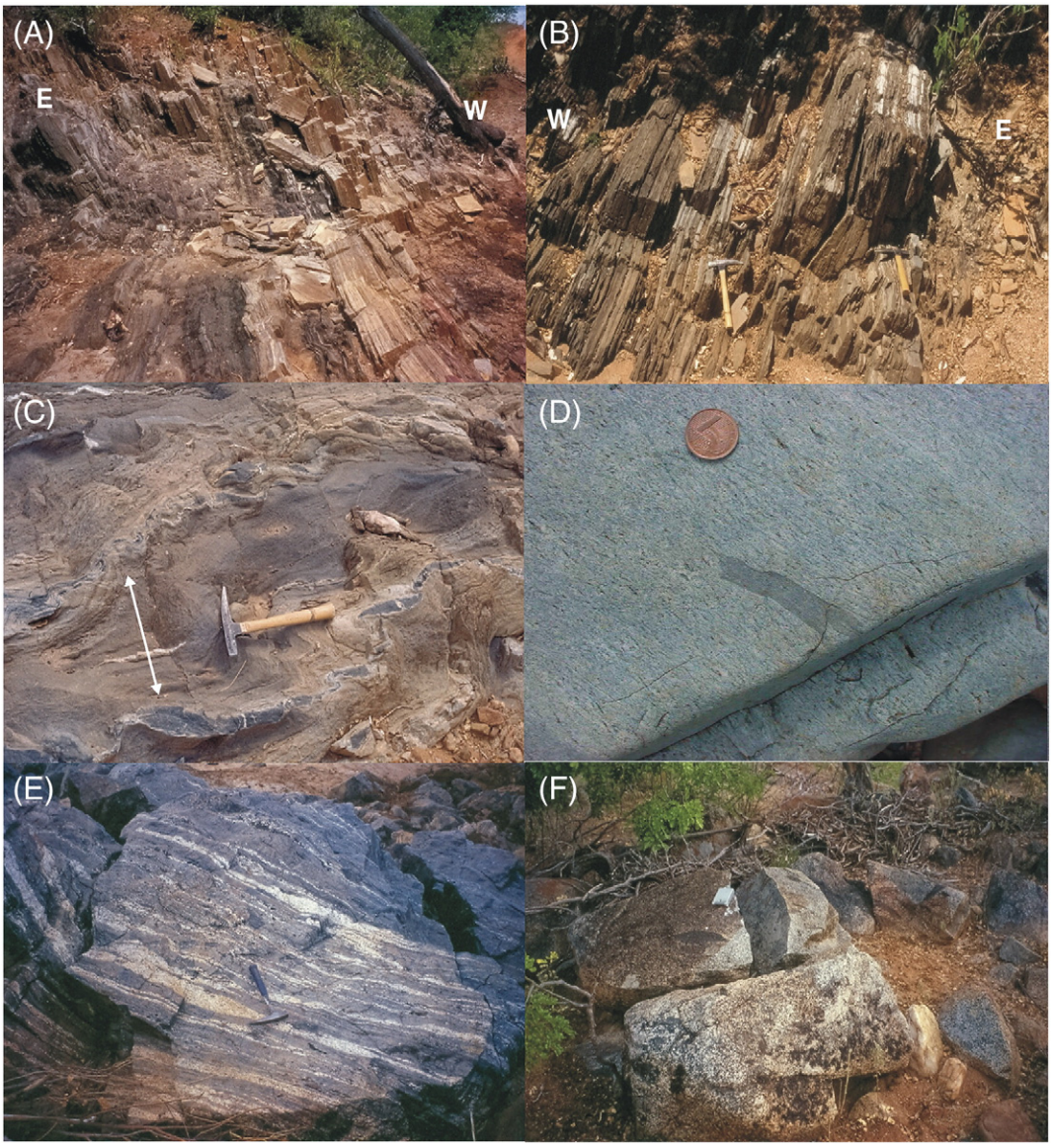

Fig. 4. Field aspects of rocks of the Rio Capim belt. A) Banded mylonites along the Galo do Ouro shear zone that separates the Uauá block and the Rio Capim belt; B) fine-grained and deformed amphibolite (metabasalt); C) sills of metadacite (arrow) in low-grade pelitic metasedimentary rock; D) metadacite with xenolith of deformed granitic rock; E) deformed coarse-grained gabbro, possibly layered; F) quartz–diorite–tonalite with small mafic enclaves.

eastwards into hornblende + clinopyroxene + garnet + plagioclase (An44–59), or clinopyroxene + hypersthene + hornblende + plagioclase. The composition of amphibole also changes significantly, as indicated by mineral analyses done by us with a Cameca SX50 electron microprobe of the Instituto de Geociências, Universidade de Brasília, Brazil (unpublished data). Fe-hornblende dominates in the west, and tschermackitic Fe-hornblende in the east, following the amphibole nomenclature of Leake (1997). Moreover, the low-grade amphiboles exhibit higher Mg-number (55–50) and higher Si cations (7.2–6.8 per formula unit), but lower TiO_2 content (<1 wt.%) than their granulite facies counterparts (Mg# = 50–45, TiO_2 = 1–2 wt.%, Si = 6.8–6.5 per formula unit). By applying the Blundy and Holland (1990) geothermometer hornblende — plagioclase for metabasic rocks, we calculated 535–541 °C and 725–800 °C, respectively for the western and eastern portions of the belt. These temperature estimates are coherent with the amphibole compositions described above, and the mineral associations found in both regions, i.e. blue to green hornblende + preserved magmatic texture to the west; brown hornblende + low-Al clinopyroxene (Wo39–46, En32–34) + low-Al hypersthene (En43–46, Wo<1.9) in mafic rocks, sillimanite + cordierite + almandine garnet in metapelites, forsterite + periclase in marbles to the east. The strong temperature variation across the belt sequence and the diagnostic mineral parageneses permit us to characterize a low to medium-pressure–high temperature metamorphism, with a geothermal gradient of about 45 °C/km.

Subsequent folding (F_3) shaped the present structural orientation of the Rio Capim belt. This deformation phase is marked by open to tight, upright to recumbent folds with N- to NW-trending axes. S_3 is typically a crenulation cleavage, or schistosity, developed under retrograde amphibolite facies conditions as shown by amphibole around orthopyroxene in mafic granulites. Several pegmatite intrusions exhibit the same orientation and foliation of S_3, hence they are likely to be syntectonic to F_3.

The Rio Capim Belt experienced one additional deformation episode (F_4), responsible for nucleation and development of two regional scale shear zones, one of which (Galo de Ouro shear zone) separates the Rio Capim belt from the Uauá block. The Galo do Ouro shear zone presents a sigmoidal S-shape, with width varying from 20 to 25 m in the north to 500 m in the south. Detailed field and microstructural studies of Souza (1986) demonstrated that the shear zones are sub-vertical, show right-lateral sense of movement, and originated by progressive heterogeneous simple shearing under greenschist to low-*T* amphibolite facies conditions. Souza (1986) suggested that F_3 and F_4 are progressive.

No geochronological study has been done for the Rio Capim belt before. However, Jardim de Sá et al. (1984) suggested an age of 3.2 Ga based on a Rb–Sr isochron of Mascarenhas and Sá (1982) for a tonalite body cropping out in the Uauá block, on the NW contact with the Rio Capim belt, close to the Galo do Ouro shear zone. This tonalite entrains amphibolite enclaves which were interpreted by Jardim de Sá et al. (1984) as metabasalts of the Rio Capim belt. Bastos Leal et al. (1994) studied two mylonitic mafic dykes of the Uauá block, close to the Galo do Ouro shear zone. Their K–Ar data yield ages of 2003 ± 86 Ma and 1975 ± 2 Ma suggesting that the F_4 above is Palaeoproterozoic in age.

4. Sampling

For this study, we selected representative samples of mafic and felsic igneous rocks, and metasedimentary rocks. Nine amphibolite facies metadacites from the Rio Capim belt and eight felsic dykes intrusive into the Uauá block were dated by the whole-rock Pb–Pb isochron technique, whereas one granulite facies leucogabbro (96-6) and another high-grade diorite (96-5.4) had their single zircon grains analysed by the thermal ionization mass spectrometry. Additional zircon grains from one metadacite (CR-3) and one high-grade quartz diorite–tonalite body (C-10) were dated by the sensitive high-resolution ion microprobe (SHRIMP). Eleven samples of several rock types (two metadacites, one metadacite dyke, two amphibolites, two metapelites, one basement felsic dyke, one leucogabbro, one diorite, and one tonalite) were chosen for Nd isotope geochemistry. Finally, fifteen metadacite and fifteen mafic rocks were also analysed for major and trace element for geochemical characterization.

Locations of the samples are shown in Fig. 3. The analytical techniques and results are presented below.

5. Analytical techniques and results

5.1. Pb–Pb isotope data

The whole-rock Pb–Pb isochron technique followed the procedures of Lafon et al. (1993). The analytical work and mass spectrometer data acquisition were all carried out in the isotope laboratory at Centro de Geociências of the Federal University of Pará, northern Brazil.

The whole-rock Pb–Pb results for metadacite volcanics and dykes are presented in Table 1 and the isochrons shown in Fig. 5. Nine samples of metadacites yielded a Pb–Pb isochron age of 2153 ± 79 Ma, whereas seven samples of felsic dykes intrusive into the Uauá block, to the west of the Rio Capim belt, yielded the age of 2218 ± 170 Ma.

5.2. SHRIMP U–Pb data

To improve the age of the Rio Capim metadacite and to have age information about granites of the Rio Capim belt, we have determined the U–Pb isotopic ages for zircon grains from the metadacite CR-3 and the quartz–diorite C-10.

Zircon crystals were mounted in epoxy with chips of the CZ3 standard zircon (564 Ma Sri Lankan zircon with 551 ppm U; Pidgeon et al., 1994; Nelson, 1997). After optical observations under a polarizing microscope, selected zircon grains were imaged on a SEM (Scanning Electron Microscope) for analysis of morphology and internal structure. U–Pb analyses were obtained using the Perth Consortium SHRIMP based on the operation procedure described by Compston et al. (1984) and operation conditions described by Smith et al. (1998). In separate analytical sessions, seven analyses of the CZ3 standard indicated a Pb/U calibration reproducibility (1σ) of 1.42% for the Rio Capim tonalite data and six analyses of the CZ3 standard indicated 1.08% reproducibility for the Rio Capim metadacite data. Common-Pb corrections were made assuming Broken Hill common-Pb compositions for all sample analyses.

The age-populations reported here are for $^{207}Pb/^{206}Pb$ with between 95% and 105% concordance. Pooled ages are quoted with

Table 1
Whole-rock Pb–Pb isotope data for rocks of the Rio Capim belt.

Sample	$^{206}Pb/^{204}Pb$	1σ	$^{207}Pb/^{204}Pb$	1σ	$^{208}Pb/^{204}Pb$	1σ
Felsic dykes in the Uauá block						
96-12	16.509	0.01	15.320	0.0139	35.692	0.043
96-13	16.036	0.0096	15.250	0.0137	35.320	0.042
MU-1	17.874	0.011	15.538	0.0142	36.522	0.044
MU-2	19.221	0.012	15.702	0.0144	37.234	0.045
MU-3.1	16.146	0.0099	15.312	0.0139	36.067	0.0438
MU-3.2	16.916	0.0102	15.419	0.0139	36.083	0.0435
MU-11	17.081	0.018	15.467	0.0232	36.890	0.088
Metadacite of the Rio Capim belt						
96.9.1	20.071	0.012	15.995	0.0144	39.309	0.048
96.9.2	18.995	0.011	15.842	0.0141	38.290	0.046
96.9.3	20.206	0.012	16.034	0.0144	38.475	0.046
96.9.4	19.801	0.012	15.962	0.0145	39.148	0.048
96.9.5	19.150	0.012	15.871	0.0148	38.428	0.049
96.9.6	19.849	0.012	15.982	0.0144	38.903	0.047
CR-1	20.150	0.012	16.009	0.0144	39.035	0.047
CR-2	22.146	0.013	16.275	0.0145	41.495	0.05
CR-3	19.586	0.016	15.976	0.0177	39.008	0.056

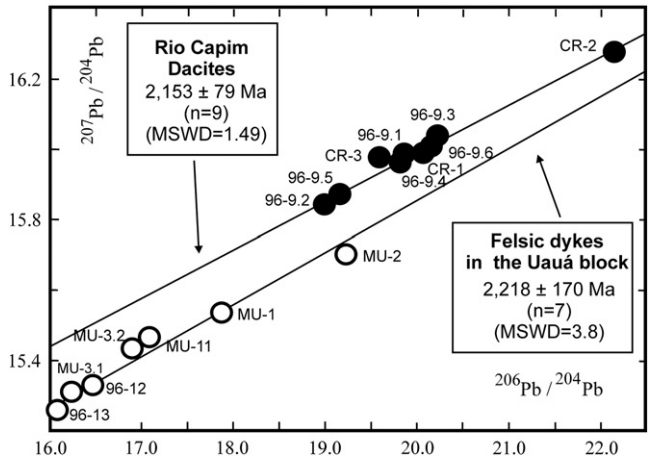

Fig. 5. Whole-rock Pb–Pb isochrons for metadacites of the Rio Capim belt and felsic dykes in the Uauá block. Analytical uncertainty (95% c.l.) similar to symbol size.

95% confidence level errors. Dates from analyses that are <95% concordant were regarded as minimum ages.

A total of 7 analyses were obtained on 7 zircon crystals from the Rio Capim metadacite and 11 analyses on 8 crystals from the Rio Capim quartz–diorite. The results are listed in Table 2 and displayed in Figs. 6 and 7, respectively. Analyses outside the $\pm 2\sigma$ interval of the mean ages of identified populations were not in the age calculation. Concordia diagrams were obtained following the procedures of Ludwig (1999).

As shown in Fig. 6 zircon crystals of the metadacite CR-3 are prismatic and show oscillatory zoning typical of felsic igneous rocks. The weighted age calculated for 7 grains was 2148 ± 9 Ma, which is fairly similar to the age obtained by the Pb–Pb isochron. For the quartz–diorite C-10 (Fig. 7) the calculated age for 5 grains was 2128 ± 7 Ma, i.e. circa 20 m.y. younger than the metadacite age above. In this rock we found a 92% discordant zircon (spot 3-2) with the $^{207}Pb/^{206}Pb$ age of 2318 ± 13 Ma and another 99% concordant grain (spot 6-1) with the single $^{207}Pb/^{206}Pb$ age of 2236 ± 5 Ma, which we interpret as inherited from older crust. This latter age is of particular regional relevance because it is similar to the Pb–Pb isochron age obtained for the metadacite dykes in the Uauá block and to populations of detrital zircon grains in metasedimentary rocks of the Rio Itapicuru greenstone belt farther to the south, for which no source has been found so far.

5.3. U–Pb isotope data

Zircon U–Pb data using a VG Sector multi-collector thermal ionization mass spectrometer (TIMS) were obtained at the Isotope Geochemistry Laboratory of the University of Kansas, USA. Abraded and non-abraded fractions of zircons were spiked with a mixed ^{205}Pb–^{235}U tracer solution and dissolved in HF and HCl in microcapsules, using procedures modified after Krogh (1973). During these analyses, analytical blanks varied from 5 to 25 pg for Pb. PBDAT (Ludwig, 1982) and ISOPLOT (Ludwig, 1999) were used to reduce raw mass spectrometer data; correct for blanks; and calculate uncertainties, concordia intercepts, and weighted averages.

Zircon crystals from the leucogabbro (96-6) are brown, fully transparent and rounded. The diorite (96-5.4), on the other hand, contains normal, white-yellow euhedral zircon grains. The results are presented in Table 3 and displayed on Fig. 8. Four zircon grains from the diorite yielded a discordia line with the upper intercept age at 2144 ± 17 Ma, whereas five grains from the leucogabbro yielded an age of 2143 ± 22 Ma. The two ages are similar and within error limits coincide with that of the metadacite above (2148 ± 9 Ma). In summary, at about 2150 Ma both mafic and felsic magmas were generated to form the continental crust of the Rio Capim belt.

5.4. U–Th–Pb electron microprobe monazite data

Monazite is a common mineral in metamorphic rocks derived from Al-rich sediments such as cordierite–garnet metapelites associated with low- and high-grade basic rocks of the Rio Capim belt. Dating monazite grains will provide time constraints for the metamorphism and deformation that affected the belt. The electron microprobe dating of monazite is now a widely used technique (Montel et al., 1996; Cocherie et al., 1998; Souza et al., 2006).

The monazite crystals were analysed for U, Th and Pb with a Camebax Micro electron microprobe of the Université Blaise Pascal, Clermont-Ferrand, with an accelerating voltage of 15 kV and a 90–145 nA probe current. The standards used were ThO_2, UO_2, and a synthetic glass ($CaO–Al_2O_3–SiO_2$) with 6200 ppm of Pb. The counting time for standards is 50 s on peak and 100 s on background for ThO_2

Table 2
Zircon SHRIMP U–Pb data of the Rio Capim metadacite CR-3 and quartz-diorite C-10.

Grain spot	U (ppm)	Th (ppm)	Th/U	4f206 (%)	204-corrected isotopic ratios										%conc	$^{207}Pb/^{206}Pb$ age (Ma)
					$^{207}Pb/^{206}Pb$	±	$^{208}Pb/^{206}Pb$	±	$^{206}Pb/^{238}U$	±	$^{207}Pb/^{235}U$	±	$^{208}Pb/^{232}Th$	±		
CR-3, Rio Capim metadacite (UWA mount A75A)																
2-1	428	201	0.471	0.211	0.1330	0.0006	0.1314	0.0010	0.3629	0.0031	6.6530	0.0673	0.1013	0.0012	93	2138 ± 8
3-1	171	57	0.332	0.054	0.1327	0.0008	0.0932	0.0011	0.3872	0.0039	7.0844	0.0879	0.1086	0.0019	99	2134 ± 10
4-1	446	177	0.396	0.085	0.1342	0.0005	0.1128	0.0008	0.3623	0.0032	6.7060	0.0672	0.1032	0.0012	93	2154 ± 7
5-1	354	173	0.489	0.012	0.1336	0.0005	0.1396	0.0008	0.3885	0.0034	7.1556	0.0720	0.1110	0.0012	99	2146 ± 7
6-1	211	172	0.816	0.079	0.1347	0.0007	0.2324	0.0016	0.3879	0.0036	7.2021	0.0815	0.1105	0.0014	98	2160 ± 9
8-1	297	133	0.446	0.411	0.1359	0.0020	0.1245	0.0027	0.3699	0.0072	6.9303	0.1806	0.1033	0.0034	93	2175 ± 26
9-1	192	83	0.431	0.056	0.1340	0.0007	0.1196	0.0013	0.3830	0.0036	7.0742	0.0814	0.1063	0.0016	97	2151 ± 9
C-10, Rio Capim quartz–diorite–tonalite (UWA mount A75B)																
1-1	63	76	1.22	0.053	0.1326	0.0012	0.3439	0.0032	0.3550	0.0047	6.4887	0.1105	0.1004	0.0018	92	2132 ± 16
2-1	82	102	1.24	0.010	0.1321	0.0012	0.3467	0.0030	0.4007	0.0053	7.2953	0.1234	0.1117	0.0020	102	2126 ± 16
3-1	56	91	1.63	0.036	0.1340	0.0021	0.4682	0.0061	0.3395	0.0049	6.2714	0.1428	0.0973	0.0021	88	2151 ± 28
3-2	188	120	0.63	0.057	0.1476	0.0012	0.1779	0.0016	0.3923	0.0053	7.9809	0.1320	0.1100	0.0021	92	2318 ± 13
4-1	123	183	1.49	0.090	0.1346	0.0033	0.3972	0.0105	0.2582	0.0058	4.7921	0.1705	0.0688	0.0027	69	2159 ± 43
5-1	133	76	0.58	0.469	0.1380	0.0013	0.1229	0.0027	0.3304	0.0043	6.2868	0.1071	0.0706	0.0019	84	2202 ± 16
5-2	46	85	1.86	0	0.1312	0.0015	0.5569	0.0057	0.3545	0.0061	6.4145	0.1385	0.1061	0.0024	93	2115 ± 20
6-1	329	250	0.76	0.006	0.1407	0.0004	0.2127	0.0011	0.4098	0.0041	7.9493	0.0871	0.1144	0.0014	99	2236 ± 5
6-2	86	110	1.29	0.081	0.1323	0.0013	0.3640	0.0035	0.3807	0.0048	6.9426	0.1188	0.1076	0.0019	98	2128 ± 18
7-1	54	58	1.07	0	0.1329	0.0011	0.3039	0.0033	0.3865	0.0052	7.0820	0.1189	0.1100	0.0021	99	2137 ± 15
8-2	71	82	1.15	0.143	0.1291	0.0022	0.3096	0.0055	0.4114	0.0082	7.3235	0.2043	0.1108	0.0034	106	2086 ± 30

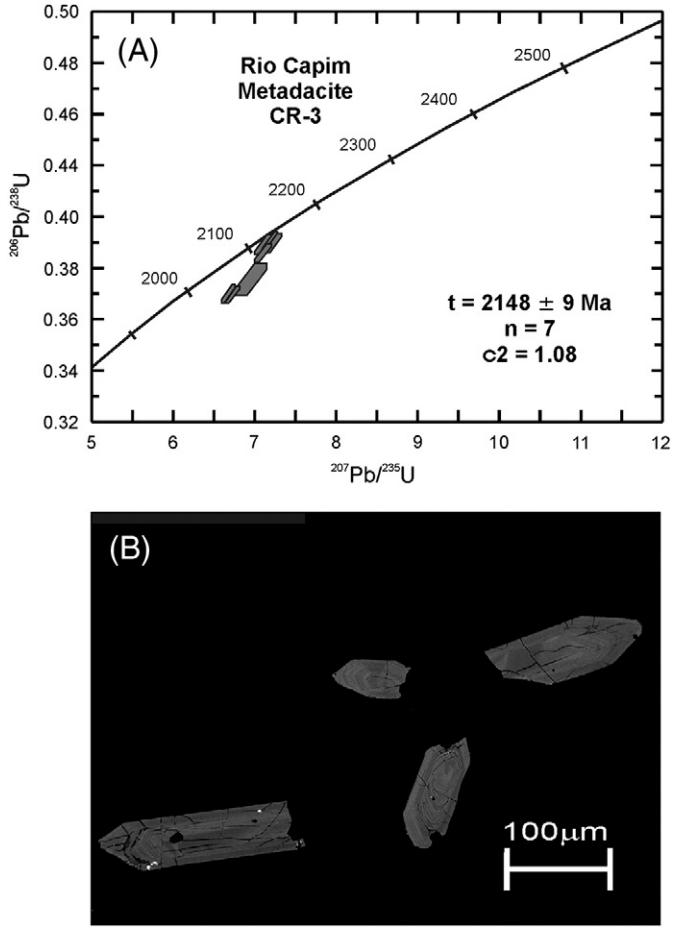

Fig. 6. (A) SHRIMP U–Pb data for the Rio Capim dacite; (B) Back-scatter electron microscope image of zircon grains showing oscillatory zoning. Error envelopes in A are 1σ. Grey-filled symbols are single grains used for age calculation.

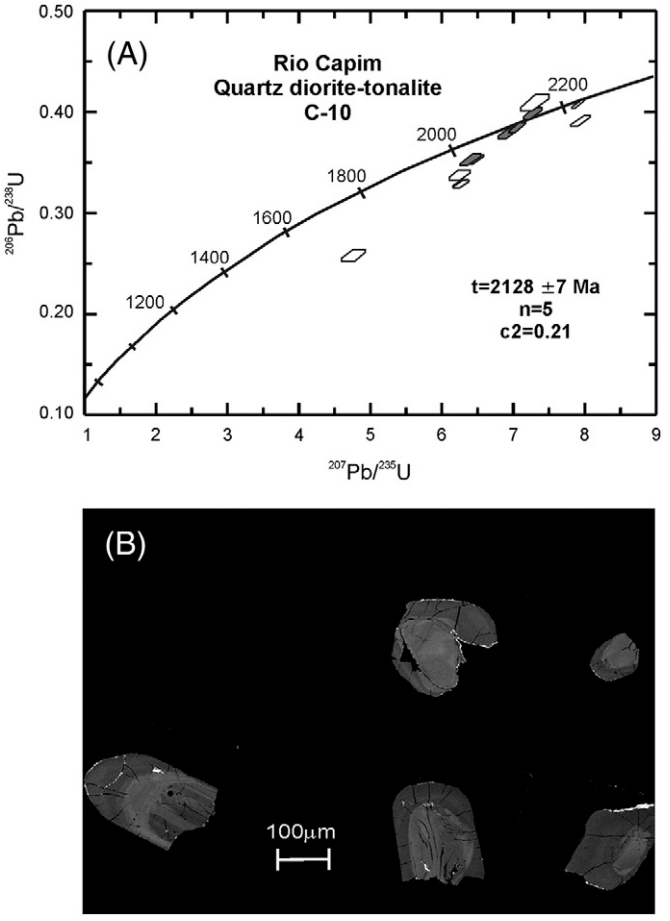

Fig. 7. (A) SHRIMP U–Pb data for the Rio Capim quartz–diorite–tonalite body; (B) Back-scatter electron microscope image of zircon grains showing oscillatory zoning. Error envelopes in A are 1σ. Grey-filled symbols are single grains used for age calculation.

an UO_2, and 300 s on peak and 600 s on background for Pb glass. For dating, the counting time was of 100 s at each point.

We analysed two samples of metapelitic rocks representative of the low- (96-8.4) and high-grade (Z-15B) zones. For the first sample, six monazite grains were analysed, and they gave an age of 2031 ± 62 Ma (2 sigma errors). For the high-grade sample, four monazite grains yielded the age of 2096 ± 69 Ma. Although the ages differ significantly from each other by 60 m.y., they are indistinguishable within the analytical error. Moreover, the ages are much younger than the ages found above for the igneous rocks and are consistent with the indicated ages for the peak of regional metamorphism in the Itabuna–Salvador–Curaçá orogen, which fall mostly in the time interval 2080–2070 Ma (Silva et al., 1997; Oliveira et al., 2002; Mello et al., 2006; Oliveira et al., 2010) but may be somewhat younger such as the 2039 ± 2 Ma found on syn-deformation titanite at the western boundary of the Uauá block (Oliveira et al., 2000).

Table 3
Isotope dilution U–Pb data for zircons of the Rio Capim diorite 96-5.4 and leucogabbro 96.6.

Mineral fraction	Weight (mg)	Concentrations			Corrected values			Age (Ma)			Rho
		U ppm	Total Pb ppm	Com Pb ppm	$^{206}Pb/^{238}U$	$^{207}Pb/^{235}U$	$^{207}Pb/^{206}Pb$	$^{206}Pb/^{238}U$	$^{207}Pb/^{235}U$	$^{207}Pb/^{206}Pb$	
96-6, Rio Capim leucogabbro											
m(5)	0.007	158.0	54.851	0.06	0.3186	5.6138	0.1278	1782	1918	2067	0.989
m(−1)	0.001	1159.3	403.56	12.20	0.3182	5.6226	0.1281	1781	1919	2072	0.994
nm(−1)−1	0.002	456.9	179.32	3.46	0.3660	6.6463	0.1317	2010	2065	2120	0.947
nm(−1)−2	0.002	587.9	228.96	0.96	0.3577	6.5216	0.1322	1971	2048	2127	0.983
nm(−1)ab	0.004	260.7	109.15	2.10	0.3782	6.8729	0.1318	2068	2095	2121	0.986
96-5.4, Rio Capim diorite											
m(0)ab	0.010	781.1	195.48	4.25	0.2196	3.5419	0.1170	1279	1536	1910	0.100
m(−1)	0.007	686.3	252.46	0.39	0.3384	6.0443	0.1295	1879	1982	2091	0.990
nm(−1)	0.007	621.9	189.18	0.50	0.2740	4.7393	0.1255	1560	1774	2035	0.995
m(−1)ab	0.002	235.3	95.96	0.95	0.3783	6.9235	0.1327	2068	2101	2134	0.993

m and nm — magnetic and non-magnetic fractions; ab — abraded grains.

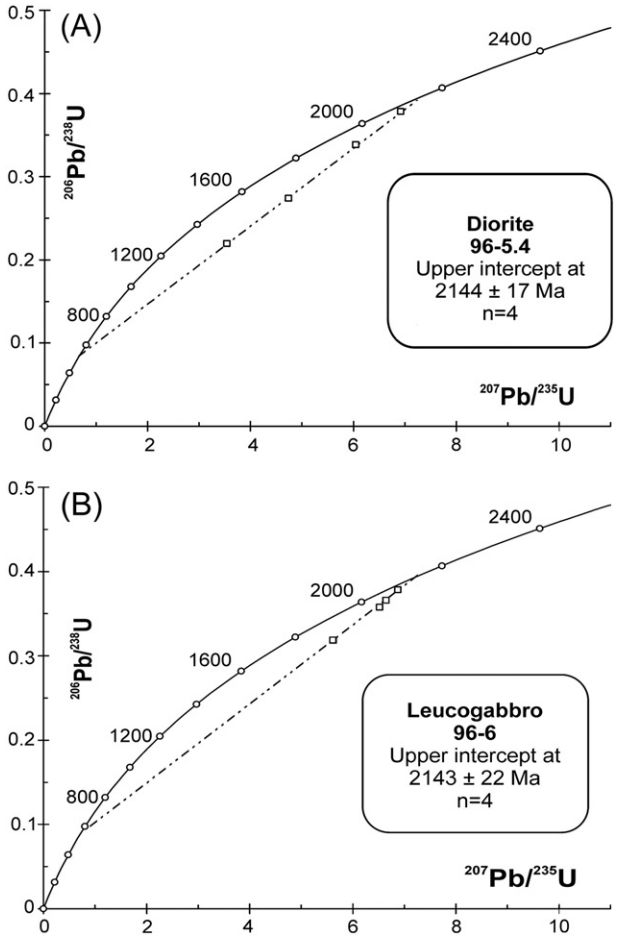

Fig. 8. TIMS U–Pb data for the (A) Rio Capim diorite (96-5.4) and (B) leucograbbro (96-6).

5.5. Sm–Nd isotope data

Sm–Nd isotopes are useful to constrain the mantle or crustal sources of igneous rocks. Sm–Nd isotope data were obtained at the Isotope Geochemistry Laboratory of the University of Kansas, USA, following the general procedures of Patchett and Ruiz (1987). Sm and Nd were loaded, respectively on Ta filament with H_3PO_4; and Re filament with H_3PO_4 and a thin coat of resin beads. Analyses were corrected for instrumental bias to a $^{143}Nd/^{144}Nd$ value for the La Jolla Nd standard of 0.511860. Correction for blanks was insignificant for Nd isotopic compositions and for Sm/Nd concentrations and ratios. Depleted mantle Nd model ages were calculated according to DePaolo (1988).

The results are shown in Table 4. The following groups are readily distinguished in order of increasing Nd model ages (TDM): metadacite dome (2.28–2.29 Ga); high-grade leucogabbro, amphibolite and granulitic diorite (2.43–2.46 Ga); low-grade amphibolite, metadacite dyke and metapelite (2.52–2.58 Ga); quartz–diorite (2.75 Ga); high-grade metapelite (3.11 Ga); Uauá block felsic dyke (3.28 Ga). These results suggest that clasts for the sediment protolith of the high-grade metapelite came from Mesoarchaean sources, possibly with minor contribution from younger sources such as the Rio Capim belt. On the other hand, the parental magma to the Uauá block felsic dykes might have originated by partial melting of the Uauá block rocks, or from younger sources with major contamination with the latter. Taking the metadacite SHRIMP U–Pb age (2148 Ma) as a reference, most rocks other than the Uauá felsic dyke, show slightly negative to positive ε_{Nd} values, suggesting a relative short crustal residence for the majority of the Rio Capim rocks and a significant juvenile contribution, especially for the metadacite flows and amphibolites.

5.6. Whole-rock geochemistry

Whole-rock major and trace elements for mafic and felsic rocks were analysed in a Philips PW2100 X-ray fluorescence spectrometer at the Geosciences Institute of the University of Campinas (UNICAMP) using respectively fusion beads and pressed powder pellets, following the procedures of Vendemiatto and Enzweiler (2001). Data quality was controlled routinely through analyses of the international reference rocks W-2 and BHVO for major elements, and RGM-1 and WSE for trace elements. The relative errors are 0.4–1.5% for major and minor elements, while for trace elements they range within 1.5–10%. Some samples were also analysed for the rare earth elements and other trace elements on a Thermo (Xseries2) quadrupole ICP-MS at the Geosciences Institute of UNICAMP following the in house adapted analytical procedures of Eggins et al. (1997) and Liang et al. (2000), and instrument conditions of Cotta and Enzweiler (2009); the results are better than 10% deviation from the recommended values for the international standards BRP-1, RGM-1 and GSP-2. A few samples were analysed for the rare earth elements, Th, Hf and Co by instrumental neutron activation analysis (INAA) at the Research Institute for Nuclear Energy (IPEN) of the University of São Paulo, following the analytical procedures of Figueiredo and Marques (1989). The accuracy and precision of the method were verified by the analysis of the reference materials granite GS-N and basalt BE-N, showing analytical precision and relative errors better than 10%. The results are listed in Table 5 and shown in Figs. 9–14.

On the total alkalis vs. silica diagram (Fig. 9a), the amphibolites, high-grade leucogabbro and diorite plot mainly in the basalt field, with four samples plotting in the fields of basaltic andesite to andesite. The metadacites have higher silica abundance and fall in the fields of dacite to rhyolite; the two metadacites that were emplaced as sill and

Table 4
Sm–Nd isotope data for rocks of the Rio Capim belt.

Sample	Rock type	Age (Ma)	Sm (ppm)	Nd (ppm)	$^{147}Sm/^{144}Nd$	$^{143}Nd/^{144}Nd$ ($\pm1\sigma$)	TDM (Ga)	$\varepsilon_{Nd}(0)$	$\varepsilon_{Nd}(T)$
CR-2[a]	Metadacite	2148	1.930	12.315	0.09475	0.511245 (11)	2.30	−27.17	0.97
CR-3[a]	Metadacite	2148	1.892	12.019	0.09516	0.511258 (11)	2.29	−26.92	1.11
Z10.B[a]	h-grade amphibolite	2143	2.005	6.407	0.18922	0.512654 (14)	2.44	0.3	2.38
Z14[a]	h-grade leucogabbro	2143	2.314	13.461	0.10395	0.511287 (15)	2.43	−26.36	−0.82
96-5.1[a]	h-grade diorite	2144	4.971	29.561	0.10168	0.511230 (15)	2.46	−27.46	−1.3
96-8.3[a]	l-grade amphibolite	2143	2.332	7.445	0.18939	0.512637 (12)	2.58	−0.02	2.0
96-8.4[a]	l-grade metapelite		4.814	25.680	0.11334	0.511380 (14)	2.52	−24.54	−1.54
96-8.5[a]	metadacite dyke	2148	4.313	24.446	0.10666	0.511259 (14)	2.54	−26.9	−2.06
C-10	Capim qtz-diorite	2128	3.48	19.964	0.10540	0.511088 (17)	2.75	−30.24	−5.3
Z15.B[a]	h-grade metapelite		3.586	13.411	0.16167	0.511998 (13)	3.11	−12.48	−2.83
MU-3.1[a]	Uauá block felsic dyke	2218	1.523	6.665	0.13815	0.511435 (12)	3.28	−23.46	−6.82

[a] Data from Lawrence (USA). Remaining from UnB (Brazil).

Table 5
Whole-rock major and trace element data for representative rocks of the Rio Capim belt.

Sample	CF1	CF3	CF5	CF5-2	CF6	CF7b	CF8	CF12	CF14	CF15	CR-1	CR-2	CR-3	96-8.2	96-8.5
Rock	Dacite	Dacite	Dacite	Dacite	Dacite	Dacite sill	Dacite	Dacite	Dacite	Dacite	Dacite	Dacite	Dacite	Dacite sill	Dacite dyke
SiO_2	71.08	69.89	70.83	70.56	70.82	71.36	70.98	70.97	70.87	71.07	70.99	71.02	71.40	69.70	67.77
TiO_2	0.32	0.33	0.32	0.32	0.33	0.33	0.31	0.33	0.32	0.33	0.30	0.31	0.30	0.63	0.75
Al_2O_3	14.80	15.43	14.95	14.94	14.81	14.94	14.72	14.81	14.88	14.75	14.26	14.36	14.51	17.79	14.42
Fe_2O_3	2.22	1.95	2.20	2.29	2.35	2.30	2.27	2.23	2.26	2.19	2.26	2.55	2.24	4.65	6.23
MnO	0.03	0.03	0.03	0.00	0.03	0.04	0.00	0.04	0.03	0.03	0.03	0.03	0.02	0.01	0.08
MgO	1.07	0.85	0.85	0.85	0.90	1.24	0.85	0.85	0.81	0.83	0.82	1.03	0.73	2.98	2.36
CaO	2.28	2.41	2.78	2.73	3.18	2.14	2.40	2.85	2.45	2.37	2.53	3.00	2.33	1.03	3.67
Na_2O	4.57	4.30	4.50	4.50	4.57	4.60	4.66	4.46	4.60	4.69	4.34	4.32	4.44	0.78	1.88
K_2O	1.89	2.96	2.01	1.99	1.43	2.36	2.08	2.12	2.24	2.00	1.97	1.33	1.67	0.34	1.45
P_2O_5	0.10	0.00	0.09	0.09	0.09	0.09	0.10	0.09	0.09	0.09	0.10	0.10	0.10	0.09	0.13
LOI	1.42	1.66	1.64	1.64	1.47	0.72	1.35	0.93	1.80	1.56	1.57	1.40	1.24	1.50	1.87
Sum	99.77	99.80	100.20	99.91	99.98	100.12	99.72	99.68	100.35	99.90	99.17	99.44	98.99	99.50	100.61
Trace elements in ppm (XRF)															
Cr	13	13	13	21	14	13	11	14	16	19	18	23	17	107	181
Ni	4.0	3.6	3.8	2.4	5.1	2.3	2.7	4.6	3.2	2.8	4.0	4.0	5.0	47.0	62.0
V	24	24	24	26	26	28	22	27	24	23	25	24	25	110	120
Cu	5	9	8	6	7	11	7	16	6	12	–	–	–	–	–
Zn	30	30	47	47	52	33	43	94	47	47	57	41	46	56	72
Rb	56	68	62	61	60	63	67	67	60	56	67	60	64	17	59
Ba	610	961	530	558	482	974	601	601	613	922	579	391	591	150	656
Sr	224	256	219	218	334	301	186	234	265	244	259	230	240	101	205
Ga	18	19	17	18	18	20	17	17	18	18	–	–	–	–	–
Nb	3.4	3.2	3.4	3.2	3.5	3.2	3.2	3.6	3.3	3.4	3.8	4.0	3.7	5.0	6.0
Zr	127	136	128	126	127	129	128	131	131	128	130	132	131	155	201
Y	3.4	3.6	3.5	3.3	5.2	5.2	3.4	3.6	3.5	3.6	3.3	3.7	3.4	20.0	19.0
Trace elements in ppm (ICP-MS or INAA)															
	ICP-MS	ICP-MS	ICP-MS	ICP-MS					ICP-MS	ICP-MS			ICP-MS	ICP-MS	ICP-MS
Li	85.0	43.0	51.0	24.5					37.0	32.9			30.8	6.4	53.3
Sc	4.0	3.0	4.0	3.2					3.0	3.5			3.4	20.8	16.5
Co	5.0	5.0	5.0	5					5.0	5			8	13	19
Nb	3.0	3.4	3.1	3.4					3.0	3.4			3.2	5.2	7
Mo	0.4	0.8	0.4	0.4					0.4	0.4			0.1	0.3	0.2
Cs	3.6	3.5	3.5	2.8					2.8	2.2			3.5	0.6	3.2
La	21.11	16.94	19.99	20.4					20.4	21.2			21	37.1	35.6
Ce	34.68	21.89	37.23	37.5					34.3	36.4			36	70.4	65.3
Pr	3.61	3.02	3.56	3.8					3.4	3.6			3.5	7.5	7
Nd	12.34	10.42	12.10	13					11.8	12.6			12.3	28.2	25.2
Sm	1.99	1.74	2.04	2.1					2.0	2			2	5.2	4.5
Eu	0.54	0.52	0.59	0.61					0.5	0.62			0.6	0.95	1.09
Gd	1.39	1.27	1.44	1.45					1.4	1.39			1.34	4.4	3.66
Tb	0.17	0.15	0.17	0.18					0.2	0.17			0.17	0.66	0.57
Dy	0.86	0.77	0.86	0.87					0.8	0.82			0.8	3.72	3.35
Ho	0.15	0.13	0.14	0.15					0.1	0.14			0.14	0.73	0.68
Er	0.37	0.34	0.38	0.38					0.3	0.36			0.34	1.97	1.89
Tm	0.05	0.05	0.05	0.05					0.1	0.05			0.05	0.3	0.29
Yb	0.33	0.29	0.33	0.34					0.3	0.29			0.3	1.94	1.91
Lu	0.05	0.05	0.05	0.05					0.0	0.04			0.04	0.29	0.29
Hf	3.60	3.50	3.70	3.34					3.7	3.34			3.08	4.72	5.39
Ta	0.3	0.3	0.3	0.3					0.3	0.3			0.3	0.6	0.7
W	0.3	0.2	0.9	0.5					0.2	0.6			0.6	0.4	2
Pb	11.2	12.4	13.2	24.4					14.8	12.9			13.7	35.3	34.8
Th	8.00	6.40	8.10	7.88					7.6	7.77			7.56	15.65	18.06
U	1.80	1.30	1.60	2.1					1.8	1.89			2.21	4.31	2.42

dyke into metapelitic rocks have the lowest silica contents amongst the felsic volcanics. In the silica vs. K_2O diagram for arc volcanics (Fig. 9b) the samples follow mostly the medium-K calc-alkaline trend; in this diagram, one andesite has high-K content and plots in the shoshonite field, whereas another andesite (CF9) and one metadacite dyke (96-8.2) plot in the low-K tholeiite field. Because the alkalis and silica are mobile elements during sub-solidus processes, the use of less mobile elements is more appropriate for metamorphosed igneous rocks. The Th vs. Co (Hastie et al., 2007) and Nb/Y vs. Zr/TiO_2 (Winchester and Floyd, 1977) diagrams are currently the best proxies for the total alkalis–silica and K_2O–Silica diagrams. As shown in Fig. 10a, the basic rocks span the fields of basalt, basaltic andesite and andesite, whereas the more evolved rocks are classified as andesite to dacite and trachy-andesite. On the Th–Co diagram (Fig. 10b) the mafic rocks are mostly calc-alkaline basalts to basaltic andesites and andesites, whereas the felsic rocks are high-K andesite to dacite. The association of basalt, basaltic andesite, andesite and dacite is typical of oceanic arcs (Condie, 1997). Conversely, continental arcs, such as the Andes, have much higher abundance of the more evolved rocks.

The arc geochemical signature of the Rio Capim samples can be further explored on the mantle-normalised multi-element diagram (spidergram) and on tectonic setting discrimination diagrams.

CF9	Z5	Z5A	Z7	Z10A	Z10B	96-8.1	96-8.1A	96-8.3	Z14.1	Z14.2	Z16.1	Z16.2	96-5.1	96-5.2
Andesite	Amphi-bolite	Amphi-bolite	Amphi-bolite	Amphi-bolite	Amphi-bolite	Amphi-bolite	Amphi-bolite	Amphi-bolite	Leuco-gabbro	Gabbro	Mafic granulite	Mafic granulite	Mafic granulite	Mafic granulite
62.25	59.47	50.76	49.73	49.18	50.33	51.12	50.82	50.64	49.13	49.29	51.32	59.87	51.66	55.39
0.76	0.84	0.97	1.38	0.98	1.01	1.24	1.26	1.16	0.99	0.94	1.13	0.63	1.09	0.76
14.96	14.71	15.37	14.89	14.29	14.91	14.71	15.10	14.40	19.86	14.66	17.60	17.09	17.82	18.40
5.92	8.88	13.11	14.90	13.08	13.48	13.80	13.82	13.38	8.88	12.68	10.30	6.22	10.08	8.44
0.10	0.14	0.22	0.22	0.20	0.22	0.21	0.22	0.20	0.14	0.21	0.13	0.09	0.15	0.12
4.25	3.65	6.17	5.15	5.98	6.25	5.47	6.21	7.19	4.85	8.08	4.79	3.01	4.71	3.47
10.27	3.67	10.21	10.01	9.99	10.22	10.05	9.84	11.40	8.55	10.49	8.97	6.79	8.94	8.79
0.96	1.55	2.57	2.32	2.10	2.33	1.98	1.86	0.80	3.16	1.20	3.87	3.87	3.83	3.91
0.13	3.79	0.41	0.47	0.83	0.84	0.38	0.37	0.27	1.42	1.22	0.94	1.18	0.98	0.68
0.16	0.14	0.10	0.12	0.09	0.09	0.13	0.12	0.11	0.38	0.07	0.26	0.15	0.25	0.18
0.72	2.35	0.63	0.64	2.78	0.85	0.48	0.79	0.59	1.87	1.51	0.54	0.36	0.64	0.35
100.47	99.19	100.52	99.83	99.50	100.53	99.57	100.41	100.14	99.23	100.35	99.85	99.26	100.15	100.49
194	290	162	164	222	75	213	196	230	112	433	123	66	94	55
99.0	69.0	50.0	39.0	74.0	33.0	61.0	78.0	75.0	37.0	113.0	66.0	18.0	66.0	29.0
121	182	286	314	182	350	256	264	279	252	332	220	89	173	178
6	–	–	–	–	–	–	–	–	–	–	–	–	–	–
51	86	106	127	102	102	110	109	97	85	100	103	74	98	81
2	192	11	10	81	34	45	12	12	80	57	18	44	27	12
247	952	151	40	611	152	246	326	163	289	324	625	1036	819	262
510	151	136	146	155	148	164	229	154	436	198	436	343	451	329
15	–	–	–	–	–	–	–	–	–	–	–	–	–	–
4.6	5.0	5.0	5.0	8.0	5.0	5.0	5.0	5.0	5.0	5.0	5.0	5.0	5.0	8.0
109	145	72	91	135	56	100	98	69	41	39	162	130	161	90
16.4	28.0	20.0	27.0	27.0	19.0	28.0	28.0	24.0	8.0	15.0	21.0	15.0	20.0	21.0
ICP-MS	INAA	ICP-MS	ICP-MS	ICP-MS	ICP-MS	ICP-MS		ICP-MS	INAA			ICP-MS	INAA	ICP-MS
12.3		8.2	5.3	30.0	10.6	11.5		7				24.8		10.8
20.7	24.5	45.4	44.6	25.0	45.4	40.7		45.9	21			17.8	26.1	21
25	32.5	46	45	29.0	45	45		51	31.4			19	33.4	25
4.1		2.7	4.9	7.8	1.8	3.2		2.1				5.7		7.1
0.2		0.2	0.5	0.6	0.1	0.2		0.3				0.3		0.3
0.6	4.4	0.8	0.1	1.4	1	1.6		1	2			0.2		0.1
13	39	4.1	13.7	30.0	4.2	10.5		5	15.3			19.8	33	22.7
31.7	73	17.5	20.8	58.0	9.9	22.7		11.7	30.2			40.9	67	49
4		1.4	3.4	6.6	1.4	2.9		1.6				4.6	8.1	6
16.8	27.3	6.9	14.7	25.0	7.1	13.3		8.2	12.55			17.6	29	24.1
3.6	5.7	2.3	3.8	5.1	2.2	3.7		2.6	2.54			3.3	5	5
0.91	1.24	0.82	1.14	1.0	0.82	1.09		0.9	1.7			1.15	1.6	1.16
3.11		2.97	4.28	5.0	2.89	4.26		3.31				2.78		4.19
0.47	0.74	0.57	0.75	0.8	0.52	0.77		0.61	0.11			0.42	0.5	0.67
2.88		3.74	4.98	4.8	3.52	5.06		4.14				2.42		3.89
0.58		0.82	1.07	1.0	0.78	1.08		0.91				0.5		0.79
1.6		2.27	2.99	2.8	2.13	3		2.49				1.32		2.1
0.24		0.36	0.46	0.4	0.34	0.48		0.38				0.2		0.32
1.62	2.6	2.29	2.89	2.8	2.15	3.02		2.48	0.73			1.31	2.33	2.05
0.23	0.32	0.34	0.44	0.4	0.32	0.45		0.37	0.11			0.19	0.25	0.29
2.74	3.8	2.11	2.46	3.9	0.97	2.89		1.98	0.71			3.42	3.8	2.15
0.3	0.82	0.2	0.4	0.7	0.1	0.2		0.2				0.4	0.42	0.5
2.1		0.9	0.7	0.8	1.2	0.3		0.8				0.3		0.3
6.6		15.9	7.6	22.4	4.6	8.8		6.9				16.5		39.7
4.2	11	2.31	2.84	11.8	0.95	3.47		1.16	0.19			1.05	1.02	1.37
0.74	3.1	0.42	0.53	2.8	0.32	0.84		0.32				0.53		0.74

Fig. 11 shows spidergrams of the Rio Capim basic rocks along with the fields of basalts to andesites of intra-oceanic arcs. Both the studied samples and the arc rocks show the remarkable negative Nb anomaly and weakly fractionated rare-earth elements; the Rio Capim samples are more akin to evolved oceanic arcs such as the New Britain arc. On the La/Yb vs. Th/Ta tectonic setting discrimination diagram for basaltic rocks (Condie, 2001) with additional data for oceanic island arcs (Pearce et al., 1995; Woodhead et al., 1998), the Rio Capim basic rocks fall mostly in, or close to the field of island arc basalts (Fig. 12); the granulite facies basic rocks contrast markedly with the others by their lower Th/Ta ratios and higher La/Yb ratios. The Th/Ta ratio is more critical for arc rocks and the observed low values may be assigned to selective removal of Th during the granulite facies metamorphism that affected these rocks.

The metadacite samples show also the typical subduction-related negative Nb anomaly on the spidergram but with more fractionated rare earth patterns (Fig. 13a). As for Ti, Y and the heavy rare earth elements, two dacite groups can be identified; one with higher abundances and another with low abundances of these elements. The former group is made up of samples that occur as sills or dykes in the metapelitic rocks, and the other group comprises the remaining rocks and one sill sample (F7b) in metapelite. Because the first group is

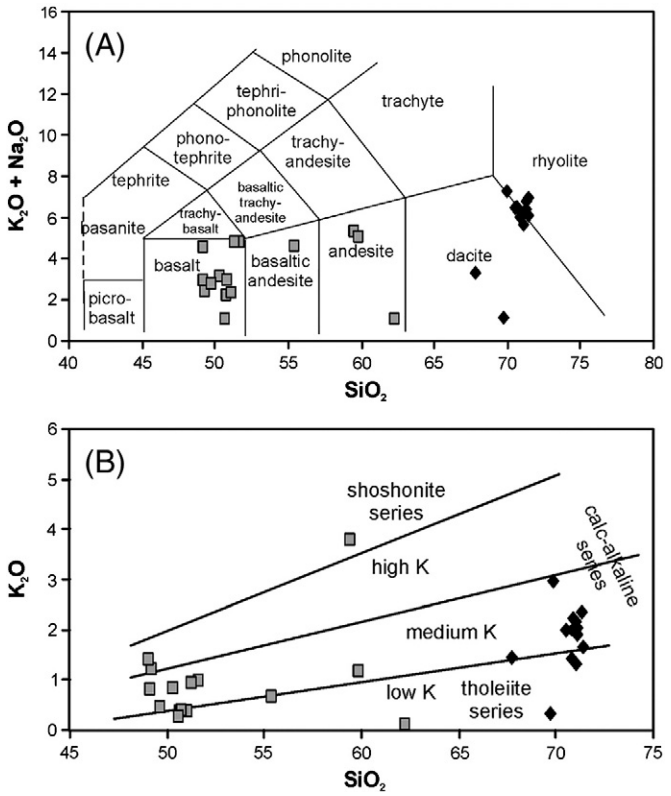

Fig. 9. Geochemical characteristics of the Rio Capim igneous rocks. A) Total alkalis vs. silica diagram with fields after Le Maitre et al. (1989); B) Silica vs. K_2O diagram for arc rocks, with fields after Peccerillo and Taylor (1976). Symbols as follows: square = mafic to intermediate rocks; losange = felsic (metadacitic) rocks.

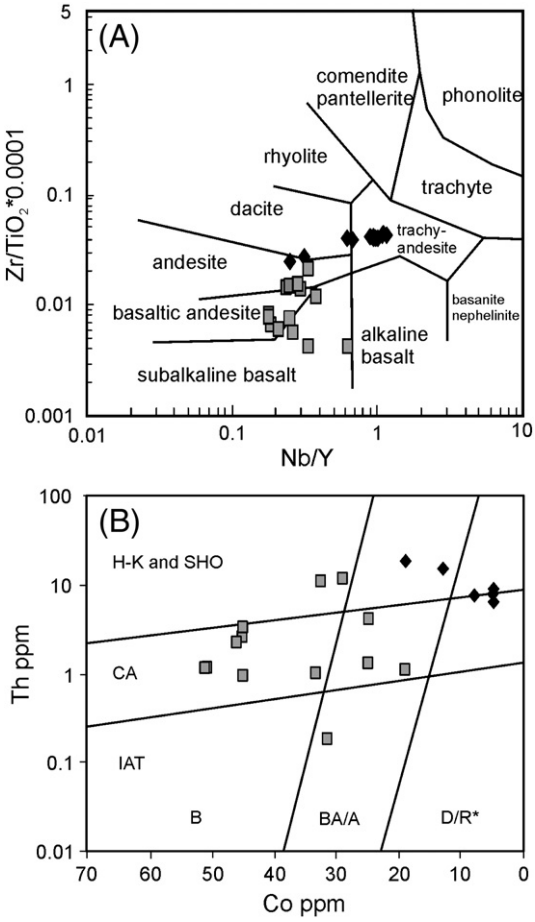

Fig. 10. Immobile trace element discrimination diagrams for classification of metaigneous rocks of the Rio Capim belt. A) Nb/Y vs. Zr/TiO_2 *0.0001 diagram of Winchester and Floyd (1977); B) Th vs. Co diagram of Hastie et al. (2007); H-K and SHO — high K_2O and shoshonite; CA — calc-alkaline; IAT — island arc tholeiite; B — basalt; BA/A — basaltic andesite and andesite; D/R — dacite and rhyolite. Symbols as in Fig. 9.

geochemicaly more primitive (high MgO and Ni, less SiO_2) and contains amphibole, fractional crystallization of this mineral (less than 30%) may account for the observed geochemical differences between the two groups (Fig. 13b).

On the granite discrimination diagram of Pearce et al. (1984) the Rio Capim metadacite samples plot all in the volcanic arc field (Fig. 14). To demonstrate that this diagram works well also for volcanic rocks, we have added data for dacites from arcs (Japan and the Andes) and intraplate rifting settings such as the Paraná continental flood basalt province (Brazil) and the Basin and Range province (USA); as shown in Fig. 14, these rocks plot in the tectonic settings they should plot, namely in the volcanic arc and within-plate fields, respectively.

In summary, the trace element geochemical signatures presented here when combined with rock association, i.e. metamorphosed basalt, andesite, dacite, gabbro, and diorite, and the positive to slightly negative epsilon Nd values of the rocks (Table 4) indicate that the most likely Phanerozoic analogue tectonic setting for the Rio Capim mafic to felsic meta-igneous rocks is the oceanic island arc.

6. Discussions and conclusions

The Rio Capim greenstone belt is composed of a rock assemblage with trace element and Nd isotope geochemical signatures that are indistinguishable from arc rocks. The dominance of basalt, andesite and dacite is more typical of oceanic rather than of continental arcs (e.g. Condie, 1997).

The new data presented here provide the basis for a tectonic model of Palaeoproterozoic arc–continent collision in the northeastern part of the São Francisco craton, in which the Rio Capim belt is a fragment of an oceanic arc and the Uauá block a remnant of the continent. The island arc sequence is represented mainly by basalt, andesite, dacite, and pelitic sedimentary rocks, and their plutonic counterparts: gabbro, diorite, quartz–diorite to tonalite, and Al-rich gneisses. During accretion, the arc sequence underwent low- to medium pressure–high temperature metamorphism and was converted into amphibolite facies rocks, in the west, and granulites in the east.

The arc may have formed in the time span 2148–2128 Ma and was likely accreted to the Archaean Uauá block between 2080 and 2070 Ma (ages of the peak of regional metamorphism), when two continental masses collided, reworked Archaean rocks, and formed the Itabuna–Salvador–Curaçá orogen. The collision was oblique as inferred from the occurrence of regional scale left-lateral strike-slip shear zones in the Serrinha block (Chauvet et al., 1997) and in the core of the orogen (Delgado et al., 2003), which eventually resulted in orogen-parallel terrane escape (Oliveira et al., 2004b, 2010). The likely lateral displacement of components of the arc and continent makes the reconstruction of the arc–continent collision zone more difficult to restore. This is particularly true for the Uauá block that is bounded to the east and west by nearly upright shear zones. Kinematic indicators along these shear zones demonstrate that the Uauá block was displaced significantly from south to north during oblique collision. As a consequence, the observed sharp contact of the Rio Capim belt with the Uauá block along the Galo do Ouro shear zone is the outcome of terrane displacement and not the original arc–continent collision zone.

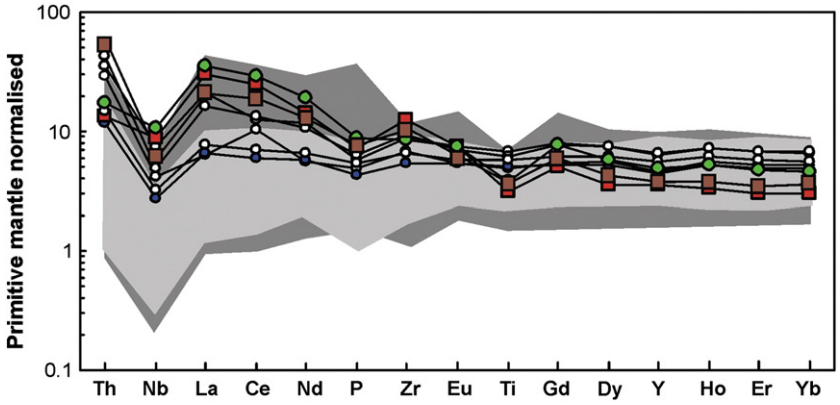

Fig. 11. Mantle-normalised, multi-element diagram for amphibolites and mafic granulites of the Rio Capim belt. Basalts and dacites of the South Sandwich arc (light grey field) and New Britain arc (dark grey field) respectively after Pearce et al. (1995) and Woodhead et al. (1998). Normalising values after McDonough and Sun (1995). Symbols as in Fig. 9.

Our interpretation of the Rio Capim belt as a fragment of an intra-oceanic arc that collided with a continental block has several additional implications.

The age of the Rio Capim arc is similar to ages of some igneous rocks in the Rio Itapicuru greenstone belt, farther to the south. The oldest rocks in this belt are 2163–2155 Ma arc plutons (Cruz Filho et al., 2005; Mello et al., 2006; Rios et al., 2009; Oliveira et al., 2010), followed by ca. 2145 Ma basalts (Oliveira et al., 2010). The basalts were intruded by a younger generation of arc-related granodiorite and tonalite (2130–2127 Ma — Chauvet et al., 1997; Mello et al., 2006) and by high-K plutons (2110–2106 Ma — Carvalho and Oliveira, 2003; Rios et al., 2007; Costa and Oliveira, 2008), the latter probably emplaced during arc–continent collision (Oliveira, 2009; Oliveira et al., 2010). The Rio Capim rocks are thus coeval with basalts and arc plutons of the Rio Itapicuru belt with ages in the time interval 2145–2127 Ma, and as such the Rio Capim belt may be a laterally displaced fragment of a major Palaeoproterozoic volcanic–sedimentary arc sequence. In this tectonic scenario, the Rio Itapicuru and the Rio Capim belts, along with the displaced Uauá block seem to belong to an accretionary orogen very much like the North American Cordilleras (e.g. Dickinson, 2009).

Juvenile magmatism in the range 2.35 to 2.1 Ga covers huge areas extending for thousands of square kilometres in the adjacent Borborema Province (Neves, 2003; Neves et al., 2006; Souza et al., 2007; Martins et al., 2009), as well as the São Luís craton to the NW (Klein et al., 2005) and French Guiana (Gruau et al., 1985; Vanderhaeghe et al., 1998; Delor et al., 2003). Similar geological and tectonic evolution is also found in Birrimian terranes in western Africa (Abouchami et al., 1990; Boher et al., 1992). It follows that the intra-oceanic and continental margin tectonics are a viable mechanism for explaining voluminous juvenile magmatism during Palaeoproterozoic times.

Finally, intra-oceanic arcs and arc–continent collision zones are potential sites for mineral exploration. Sediment-hosted massive-type sulphide occurrences are known in the Rio Capim belt (Winge, 1981) and our new model increases the prospect of new findings. Therefore, mineral exploration in the Rio Capim belt should be encouraged.

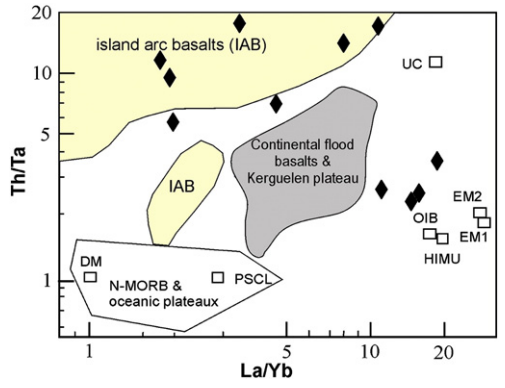

Fig. 12. Th/Ta vs. La/Yb diagram (Condie, 2001) for amphibolites and mafic granulites of the Rio Capim belt (losanges). Fields for intra-oceanic arc based on data from Pearce et al. (1995) and Woodhead et al. (1998).

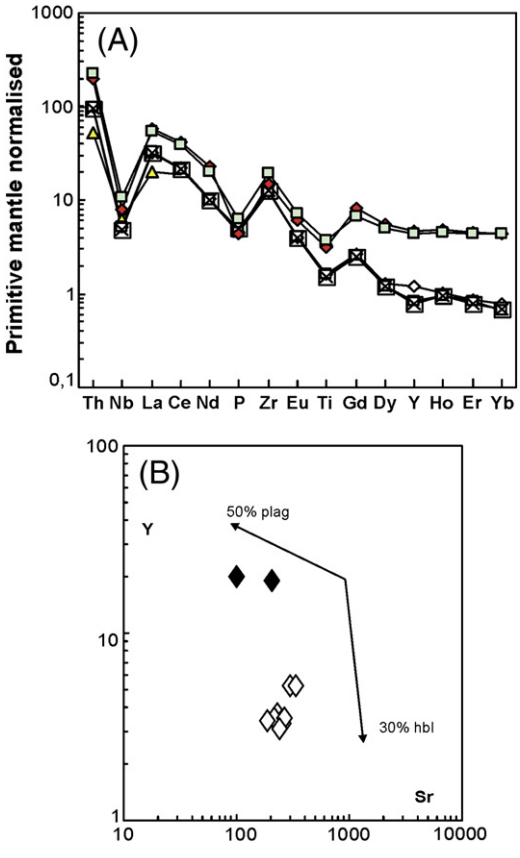

Fig. 13. Trace element characteristics of metadacites from the Rio Capim belt. A) Mantle-normalised, multi-element diagram (normalising values after McDonough and Sun, 1995); B) Fractional crystallization modeling with partition coefficients for Y and Sr for hornblende and plagioclase after Rollinson (1993). Filled losanges — sills and dykes; open losanges — lavas.

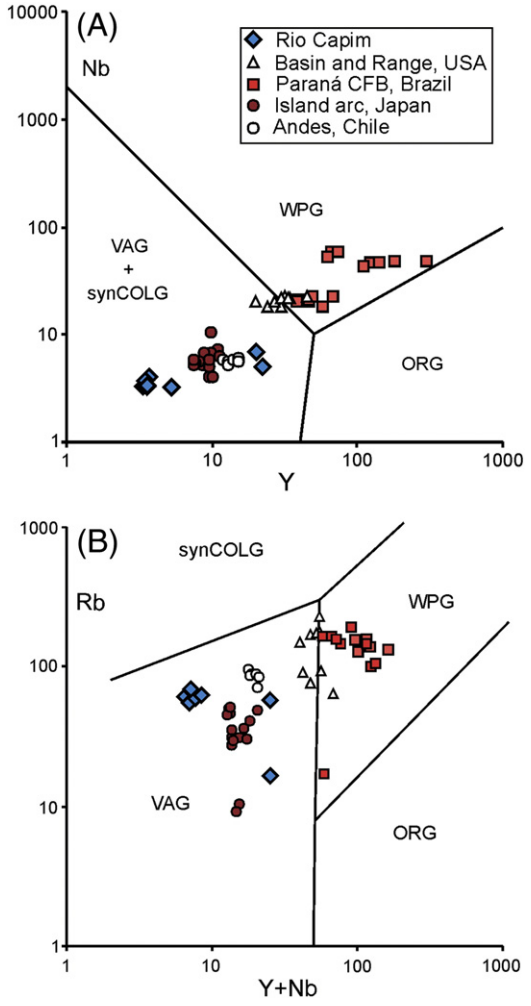

Fig. 14. Tectonic setting discrimination diagrams of Pearce et al. (1984) for metadacites of the Rio Capim belt, with additional samples of dacites from arcs (Japan — Tamura et al., 2003; Chile — Costa and Singer, 2002) and intracontinental settings (Paraná — Janasi et al., 2007; Mincato, 1994; and Basin and Range — Gans et al., 1989); syn-COLG — syn-collision granites; VAG — volcanic arc granites; WPG — within-plate granites; ORG — ocean-ridge granites.

Acknowledgments

Brian Windley read an early draft and provided useful comments and suggestions. Jean-Marc Montel, then at the Université Blaise Pascal during the post-doc leave of ZSS (1997–1998, CAPES grant 3070/95-11 and COFECUB grant 177/95), is greatly acknowledged for laboratory facilities and acquiring U–Th–Pb electron microprobe monazite data. We thank W.R. van Schmus for laboratory facilities at Kansas University, USA. SHRIMP facilities are supported by a consortium of Western Australian universities-government and ARC. The Brazilian FAPESP (96/03821-8, 06/06222-1) and CNPq (300845/91-0, 302590/2008-0) are greatly acknowledged for research grants to EPO. We benefited from the positive comments of two referees.

References

Abouchami, W.M., Boher, M., Michard, A., Albarède, F., 1990. A major 2.1 Ga event of mafic magmatism in West Africa: an early stage of crustal accretion. Journal of Geophysical Research 95, 17605–17629.

Alibert, C., Barbosa, J., 1992. Ages U–Pb déterminés à la SHRIMP sur des zircons du complexe de Jequié, craton du São Francisco, Bahia, Brésil. Societé Géologique de France, éd., 14e RST, Toulouse, Abstract, p. 4.

Ávila, C.A., Teixeira, W., Cordani, U.G., Barrueto, H.R., Pereira, R.M., Martins, V.T.S., Dunyi, L., 2006. The Glória quartz–monzodiorite: isotopic and chemical evidence of arc-related magmatism in the central part of the Paleoproterozoic Mineiro belt, Minas Gerais State, Brazil. Anais da Academia Brasileira de Ciências 78, 543–556.

Barbosa, J.S.F., 1990. The granulites of the Jequié Complex and Atlantic Mobile Belt, southern Bahia, Brazil — an expression of Archean–Proterozoic plate convergence. In: Vielzeuf, D., Vidal, P. (Eds.), Granulites and Crustal Evolution. Springer Verlag, pp. 195–221.

Barbosa, J.S.F., Sabaté, P., 2004. Archaean and Paleoproterozoic crust of the São Francisco Craton, Bahia, Brazil: geodynamic features. Precambrian Research 133, 1–27.

Barbosa, J.S.F., Oliveira, E.P., Corrêa Gomes, L.C., Marinho, M.M., Melo, R.C., 2001. I Workshop sobre o Orógeno Itabuna–Salvador–Curaçá. 10–16 de setembro 2001, Salvador, Bahia.

Barbosa, J.S.F., Peucat, J.-J., Martin, H., Silva, F.C.A., Moraes, A.M., Corrêa-Gomes, L.C., Sabaté, P., Marinho, M.M., Fanning, C.M., 2008. Petrogenesis of the late-orogenic Bravo granite and surrounding high-grade counry rocks in the Palaeoproterozoic orogen of Itabuna–Salvador–Curaçá block, Bahia, Brazil. Precambrian Research 167, 35–52.

Bastos Leal, L.R., Teixeira, W., Piccirillo, E.M., Menezes Leal, A.B., Girardi, V.A.V., 1994. Geocronologia Rb/Sr e K/Ar do enxame de diques máficos de Uauá, Bahia (Brasil). Geochimica Brasiliensis 8, 99–114.

Bignold, S.M., Treloar, P.J., 2003. Northward subduction of the Indian plate beneath the Kohistan island arc, Pakistan Himalaya: new evidence from isotopic data. Journal of the Geological Society 160, 377–384.

Blundy, J.D., Holland, T.J.B., 1990. Calcic amphibole equilibria and a new amphibole — plagioclase geothermometer. Contributions to Mineralogy and Petrology 104, 208–224.

Boher, M., Abouchami, W., Michard, A., Albarède, F., Arndt, N., 1992. Crustal growth in west Africa at 2.1 Ga. Journal of Geophysical Research 97, 345–369.

Bueno, J.F., Oliveira, E.P., McNaughton, N., Laux, J.H., 2009. U–Pb dating of granites in the Neoproterozoic Sergipano Belt, NE-Brazil: implications for the timing and duration of continental collision and extrusion tectonics in the Borborema Province. Gondwana Research 15, 86–97.

Carvalho, M.J., Oliveira, E.P., 2003. Geologia do Tonalito Itareru, Bloco Serrinha, Bahia: uma intrusão sin-tectônica do início da colisão continental no Segmento Norte do Orógeno Itabuna–Salvador–Curaçá. Revista Brasileira de Geociências 33 (1-Suplemento), 55–68.

Chauvet, A., Silva, F.C.A., Faure, M., Guerrot, C., 1997. Structural evolution of the Paleoproterozoic Rio Itapicuru granite–greenstone belt (Bahia, Brazil): the role of synkinematic plutons in the regional tectonics. Precambrian Research 84, 139–162.

Cocherie, A., Legende, O., Peucat, J.-J., Kouamelan, A.N., 1998. Geochronology of polygenetic monazites constrained by in situ electron microprobe Th–U–total lead determination: implications for lead behaviour in monazite. Geochimica et Cosmochimica Acta 62, 2475–2797.

Compston, W., Williams, I.S., Meyer, C., 1984. U–Pb geochronology of zircons from lunar breccia 73217 using a sensitive high mass-resolution ion microprobe. Journal of Geophysical Research 89, B252–B534.

Condie, K.C., 1997. Plate Tectonics and Crustal Evolution, 4th ed. Butterworth-Heinemann.

Condie, K.C., 2001. Mantle Plumes and Their Record in Earth History. Cambridge University Press.

Cordani, U. G., Teixeira, W., 2007. Proterozoic accretionary belts in the Amazonian Craton. In: Hatcher, R.D.Jr.; Carlson, M.P.; McBride, J.H.; Martínez-Catalán, J.R.. (Org.). 4-D Framework of Continental Crust. Denver, USA: Geological Society of America, v. 200, 297–320.

Cordani, U.G., Sato, K., Nutman, A., 1999. Single zircon SHRIMP determination from Archean tonalitic rocks near Uauá, Bahia, Brazil. Proceedings II South American Symposium on Isotope Geology, pp. 27–30.

Cordani, U.G., Teixeira, W., D'Agrella-Filho, M.S., Trindade, R.I., 2009. The position of the Amazonian Craton in supercontinents. Gondwana Research 15, 396–407.

Costa, F.G., Oliveira, E.P., 2008. Age and geochemistry of the Fazenda Gavião high Ba–Sr granodiorite: Implications for continental arc magmatism in the Paleoproterozoic Rio Itapicuru Greenstone Belt, São Francisco Craton, Bahia, Brazil. 33º. International Geological Congress. CD-ROM.

Costa, F., Singer, B., 2002. Evolution of Holocene dacite and compositionally zoned magma, Volcán San Pedro, Southern Volcanic Zone, Chile. Journal of Petrology 43, 1571–1593.

Cotta, A., Enzweiler, J., 2009. Quantification of major and trace elements in water samples by ICP-MS and collision cell to attenuate Ar and Cl-based polyatomic ions. Journal of Analytical Atomic Spectrometry 24, 1406–1413.

CPRM (unpublished) Provisional geological maps of Uauá and Senhor do Bonfim sheets (1:250,000). Companhia de Pesquisa de Recursos Minerais (CPRM), Salvador, Bahia-Brazil.

Cruz Filho, B.E., Conceição, H., Rosa, M.L.S., Rios, D.C., Macambira, M.J.B., Marinho, M.M., 2005. Geocronologia e assinatura isotópica (Rb–Sr e Sm–Nd) do Batólito Trondhjemítico Nordestina, Núcleo Serrinha, Nordeste do Estado da Bahia. Revista Brasileira de Geociências 35, 1–8.

Cunha, J.C., Fróes, R.J.B., 1994. Komatiítos com textura spinifex do Greenstone Belt de Umburanas, Bahia. Companhia Baiana de Pesquisa Mineral: Série Arquivos Abertos, 7. Salvador-Brasil.

Davison, I., Teixeira, J.B.G., Silva, M.G., Rocha Neto, M.B., Matos, F.M.V., 1988. The Rio Itapicuru Greenstone Belt, Bahia, Brazil: structure and stratigraphical outline. Precambrian Research 42, 1–17.

Delgado, I.M., Souza, J.D., Silva, L.C., Silveira Filho, N.C., Santos, R.A., Pedreira, A.J., Guimarães, J.T., Angelim, L.A.A., Vasconcelos, A.M., Gomes, I.P., Lacerda Filho, J.V., Valente, C.R., Perrota, M.M., Heineck, C.A., 2003. Geotectônica do Escudo Atlântico. In: Bizzi, L.A., Schobbenhaus, C., Vidotti, R.M., Gonçalves, J.H. (Eds.), Geologia, Tectônica e Recursos Minerais do Brasil. CPRM, pp. 227–334.

Delor, C., Lahondère, D., Egal, E., Lafon, J.M., Cocherie, A., Guerrot, C., Rossi, P., Truffert, C., Théveniaut, H., Phillips, D., Avelar, V.G., 2003. Transamazonian crustal growth and reworking as revealed by the 1:500,000-scale geological map of French Guiana (2nd edtion). Géologie de la France 2–4, 5–57.
DePaolo, D.J., 1988. Neodymium Isotope Geochemistry. An Introduction. Springer-Verlag.
Dickinson, W.R., 2009. Anatomy and global context of the North American Cordillera. Geological Society of America Memoirs 204, 1–29.
Eggins, S.M., Woodhead, J.D., Kinsley, L.P.J., Mortimer, G.E., Sylvester, P., McCulloch, M. T., Hergt, J.M., Handler, M.R., 1997. A simple method for the precise determination of >40 trace elements in geological samples by ICPMS using enriched isotope internal standardisation. Chemical Geology 134, 311–326.
Figueiredo, M.C.H., 1989. Geochemical evolution of eastern Bahia, Brazil: a probable Early Proterozoic subduction-related magmatic arc. Journal of South American Earth Sciences 2, 131–145.
Figueiredo, A.M.G., Marques, L.S., 1989. Determination of rare earths and other trace elements in the Brazilian Geological Standards BB-1 and GB-1 by neutron activation analysis. Geochimica Brasiliensis 3, 1–8.
Fonseca, V.P., 1986. Geologia da região de Rio Capim, Uauá-BA — Área Algodões. Relatório de Graduação, Dept. Geologia, UFRN, 191 pp.
Gans, P.B., Mahood, G.A., Schermer, E., 1989. Synextencional magmatism in the Basin and Range Province; a case study from the easten Great Basin. Geological Society of America, Special paper, 233.
Gruau, G., Martin, H., Leveque, B., Capdevila, R., 1985. Rb–Sr and Sm–Nd geochronology of Lower Proterozoic granite–greenstone terrains in French Guiana, South America. Precambrian Research 30, 63–80.
Hastie, A.R., Kerr, A.C., Pearce, J.A., Mitchell, S.F., 2007. Classification of altered volcanic island arc rocks using immobile trace elements: development of the Th–Co discrimination diagram. Journal of Petrology 48, 2341–2357.
Isozkai, Y., Aoki, K., Nakama, T., Yanai, S., 2010. New insight into a subduction-related orogen: a reappraisal of the geotectonic framework and evolution of the Japanese Islands. Gondwana Research 18, 82–105.
Janasi, V.A., Montanheiro, T.J., Freitas, V.A., Reis, P.M., Negri, F.A., Dantas, F.A., 2007. Geology, petrography and geochemistry of the acid volcanism of the Paraná magmatic province in the Piraju–Ourinhos region, SE Brazil. Revista Brasileira de Geociências 37, 745–759.
Jardim de Sá, E.F.J., Souza, Z.S., Fonseca, V.P., Legrand, J.M., 1984. Relações entre "greenstone belts" e terrenos de alto grau: o caso da faixa Rio Capim, NE da Bahia. Proceedings XXXIII Congresso Brasileiro de Geologia, Rio de Janeiro, pp. 2615–2629.
Kishida, A., Riccio, L., 1980. Chemostratigraphy of lava sequences from the Rio Itapicuru Greenstone Belt, Bahia, Brazil. Precambrian Research 11, 161–178.
Klein, E.L., Moura, C.A.V., Pinheiro, B.L.S., 2005. Paleoproterozoic crustal evolution of the São Luís craton, Brazil: evidence from zircon geochronology and Sm–Nd isotopes. Gondwana Research 8, 177–186.
Krogh, T.E., 1973. A low contamination method for hydrothermal decomposition of zircon and extraction of U and Pb for isotopic ages determinations. Geochimica et Cosmochimica Acta 37, 485–494.
Lafon, J.M., Rodrigues, E., Scheller, T., 1993. Geocronologia Pb–Pb em feldspatos e rocha total: procedimento experimental e exemplos de aplicações. 4 Congresso Brasileiro de Geoquímica, Brasilia, 1993. Resumos Expandidos, Brasilia, SBGq. , pp. 242–244.
Le Maitre, R.W., Bateman, P., Dudek, A., Keller, J., Lameyre, J., Le bas, K.J., Sabine, P.A., Schmid, R., Sorensen, H., Streckeisen, A., Woolley, A.R., Zanettin, B., 1989. A Classification of Igneous Rocks and Glossary of Terms. Blackwell, Oxford.
Leake, B.E., 1997. Nomenclature of amphiboles. Report of the subcommittee on amphiboles of the International Mineralogical Association Commission on New Minerals and Mineral Names. European Journal of Mineralogy 9, 623–651.
Ledru, P., Milési, J.P., Johan, V., Sabaté, P., Maluski, H., 1997. Foreland basins and gold-bearing conglomerates: a new model for the Jacobina Basin (São Francisco province, Brazil). Precambrian Research 86, 155–176.
Leite, C.M.M., Barbosa, J.S.F., Goncalves, P., Nicollet, C., Sabaté, P., 2009. Petrological evolution of silica-undersaturated sapphirine-bearing granulite in the Paleoproterozoic Salvador–Curaçá Belt, Bahia, Brazil. Gondwana Research 15, 49–70.
Liang, Q., Jing, H., Gregoire, D.C., 2000. Determination of trace elements in granites by inductively coupled plasma mass spectrometry. Talanta 51, 507–513.
Lobato, L.M., Rodrigues, L.C.R., Zucchetti, M., Noce, C.M., Baltazar, O.F., Silva, L.C., Pinto, C.P., 2001. Brazil's premier gold province. Part I: the tectonic, magmatic and structural setting of the Archaean Rio das Velhas greenstone belt, Quadrilátero Ferrífero. Mineralium Deposita 36, 228–248.
Ludwig, K.R., 1982. A computer program to convert raw U–Th–Pb isotope ratios to blank-corrected isotope ratios and concentrations with associated error-correlations. USGS Open-File Rep. OF-82-820.
Ludwig, K.R., 1999. Isoplot/Ex — a geochronological toolkit for Microsoft Excel. Special Publication, No. 1a. Berkeley Geochronological Center.
Martins, G., Oliveira, E.P., Lafon, J.M., 2009. The Algodões amphibolite–tonalite gneiss sequence, Borborema Province, NE Brazil: Geochemical and geocronological evidence for Palaeoproterozoic accretion of oceanic plateau/back arc basalts and adakitic plutons. Gondwana Research 15, 71–85.
Mascarenhas, J.F., 1979. Evolução geotectônica do Precambriano do Estado da Bahia. In: Inda, H.A.V. (Ed.), Geologia e Recursos Minerais do Estado da Bahia; textos básicos, v. 2. SME/CPM, Salvador, pp. 57–165.
Mascarenhas, J.F., Sá, J.H.S., 1982. Geological and metallogenic patterns in the Archean and Early Proterozoic of Bahia State, Eastern Brazil. Revista Brasileira de Geociências 12, 193–214.
McDonough, W.F., Sun, S.-S., 1995. The composition of the Earth. Chemical Geology 120, 223–253.
Mello, E.F., Xavier, R.P., McNaughton, N.J., Hagemann, S.G., Fletcher, I., Snee, L., 2006. Age constraints on felsic intrusions, metamorphism and gold mineralization in the Paleoproterozoic Rio Itapicuru greenstone belt, NE Bahia State, Brazil. Mineralium Deposita 40, 849–866.
Mincato R.L., 1994. Potential of the Paraná continental igneous province for Ni–Cu–PGE mineralisations based on the Noril'sk and Ensizwa models. Master Dissertation, Graduate course in Geosciences, State University of Campinas. (in Portuguese).
Montel, J.-M., Foret, S., Veschambre, M., Nicollet, C., Provost, A., 1996. Electron microprobe dating of monazite. Chemical Geology 131, 37–53.
Nelson, D.R., 1997. Compilation of SHRIMP U–Pb zircon geochronology data, 1996. Geological Survey of Western Australia, Rec. 1997/2. 189 pp.
Neves, S.P., 2003. Proterozoic history of the Borborema Province (NE Brazil): correlations with neighboring cratons and Pan-African belts and implications for the evolution of western Gondwana. Tectonics 22, 1031. doi:10.1029/2001TC001352.
Neves, S.P., Bruguier, O., Vauchez, A., Bosch, D., Silva, J.M.R., Mariano, G., 2006. Timing of crust formation, deposition of supracrustal sequences, and Transamazonian and Brasiliano metamorphism in the East Pernambuco belt (Borborema Province, NE Brazil): implications for western Gondwana assembly. Precambrian Research 149, 197–216.
Oliveira E.P., 2009. Arc–continent collision in the Palaeoproterozoic Rio Itapicuru greenstone belt, São Francisco craton, Brazil. In: Glen R.A. & Martin C. (compilers) International Conference on Island–Arc Continent Collisions. The Macquarie Arc Conference, April 2009, Geological Society of Australia, Abstracts No. 92, 104–105.
Oliveira, E.P., Lafon, J.-M., Souza, Z.S., 1999. Archaean–Proterozoic transition in the Uauá Block, NE São Francisco Craton, Brazil: U–Pb, Pb–Pb and Nd isotope constraints. First International Symposium on Tectonics of the Brazilian Geological Society, Lençóis-BA, 12–15 May. Abstract Volume, pp. 38–40.
Oliveira, E.P., Souza, Z.S., Corrêa Gomes, L.C., 2000. U–Pb dating of deformed mafic dyke and host gneiss: implications for understanding reworking processes on the western margin of the Archaean Uauá block, NE São Francisco Craton, Brazil. Revista Brasileira de Geociências 30, 149–152.
Oliveira, E.P., Mello, E.F., MacNaughton, N.J., 2002. Reconnaissance U–Pb geochronology of early Precambrian quartzites from the Caldeirão belt and their basement, NE São Francisco Craton, Bahia, Brazil: implications for the early evolution of the Palaeoproterozoic Salvador–Curaçá Orogen. Journal of South American Earth Sciences 15, 284–298.
Oliveira, E.P., Carvalho, M.J., McNaughton, N.J., 2004a. Evolução do segmento norte do Orógeno Itabuna–Salvador–Curaçá: cronologia da acresção de arcos, colisão continental e escape de terrenos. Boletim Geologia USP — Série Científica 4, 41–53.
Oliveira, E.P., Windley, B.F., McNaughton, N.J., Pimentel, M., Fletcher, I.R., 2004b. Contrasting copper and chromium metallogenic evolution of terranes in the Palaeoproterozoic Itabuna–Salvador–Curaçá Orogen, São Francisco Craton, Brazil: new zircon (SHRIMP) and Sm–Nd (model) ages and their significance for orogen-parallel escape tectonics. Precambrian Research 128, 143–165.
Oliveira, E.P., McNaughton, N.J., Armstrong, R., 2010. Mesoarchaean to Palaeoproterozoic growth of the northern segment of the Itabuna–Salvador–Curaçá Orogen, São Francisco Craton, Brazil. In: Kusky, T., Mingguo, Z., Xiao, W. (Eds.), The Evolving Continents: Understanding Processes of Continental Growth: Geological Society of London Special Publication, 338, pp. 263–286. doi:10.1144/SP338.13.
Paixão, M.A.P., Oliveira, E.P., 1998. The Lagoa da Vaca complex: an Archaean layered anorthosite body on the western edge of the Uauá Block, Bahia, Brazil. Revista Brasileira de Geociencias 28, 201–208.
Patchett, P.J., Ruiz, J., 1987. Nd isotopic ages of crust formation and metamorphism in the Precambrian of eastern and southern Mexico. Contribution to Mineralogy and Petrology 96, 523–528.
Pearce, J., Harris, N.B.W., Tindle, A.G., 1984. Trace element discrimination diagrams for the tectonic interpretation of granitic rocks. Journal of Petrology 25, 956–983.
Pearce, J.A., Baker, P.E., Harvey, P.K., Luff, I.W., 1995. Geochemical evidence for subduction fluxes, mantle melting and fractional crystallization beneath the South Sandwich island arc. Journal of Petrology 36, 1073–1109.
Peccerillo, R., Taylor, S.R., 1976. Geochemistry of Eocene calc-alkaline volcanic rocks from the Kastamonu area, northern Turkey. Contribution to Mineralogy and Petrology 58, 63–81.
Peucat, J.J., Mascarenhas, J.F., Barbosa, J.S., Souza, F.S., Marinho, M.M., Fanning, C.M., Leite, C.M.M., 2002. 3.3 Ga SHRIMP U-Pb zircon age of a felsic metavolcanic rock from the Mundo Novo greenstone belt in the São Francisco craton, Bahia (NE Brazil). Journal of South American Earth Sciences 15, 363–373.
Pidgeon, R.T., Furfaro, D., Kennedy, A.K., Nemchim, A.A., Bronswjk, Van, 1994. Calibration of zircon strandards for the Curtin SHRIMP II. Abstracts of the 8th International Conference on Geochronology, Cosmochronology and Isotope Geology, Berkeley, USA: U.S. Geological Survey Circular, v. 1107, p. 251.
Rios, D.C., Conceição, H., Davis, D.W., Plá Cid, J., Rosa, M.L.S., Macambira, M.J.B., McReath, I., Marinho, M.M., Davis, W.J., 2007. Palaeoproterozoic potassic–ultrapotassic magmatism: Morro do Afonso sienite pluton, Bahia, Brazil. Precambrian Research 154, 1–30.
Rios, D.C., Davis, D.W., Conceição, H., Davis, W.J., Rosa, M.L.S., Dickin, A.P., 2009. Geologic evolution of the Serrinha nucleus granite–greenstone terrane (NE Bahia, Brazil) constrained by U–Pb single zircon geochronology. Precambrian Research 170, 175–201.
Rollinson, H., 1993. Using Geochemical Data: Evaluation, Presentation, Interpretation. Longman Scientific & Technical, England.
Ruiz, A.S., Geraldes, M.C., Matos, J.B., Teixeira, W., Van Schumus, W.R., Schmitt, R.S., 2004. The 1590–1520 Ma Cachoeirinha magmatic arc and its tectonic implications for the Mesoproterozoic SW Amazonian craton crustal evolution. Anais da Academia Brasileira de Ciências 76, 807–824.

Sabaté, P., Peucat, J.-J., Melo, R.C., Pereira, L.H.M., 1994. Datação por Pb-evaporação de monozircão em ortognaisse do Complexo Caraíba: expressão do acrescimento crustal transamazônico do Cinturão Salvador–Curaçá (Cráton do São Francisco, Bahia, Brasil). 38º Congresso Brasileiro de Geologia, Camboriú, v. 1, pp. 219–220.

Safonova, I.Yu., Utsunomia, A., Kojima, S., Nakae, S., Tourtogoo, O., Filippov, A.N., Koizumi, K., 2009. Pacific superplume-related oceanic basalts hosted by accretionary complexes of Central Asia, Russian Far East and Japan. Gondwana Research 17, 587–608.

Santos, J.O.S., Breemen, O.B.V., Groves, D.I., Hartmann, L.A., Almeida, M.E., McNaughton, N.J., Fletcher, I.R., 2004. Timing and evolution of multiple Paleoproterozoic magmatic arcs in the Tapajós Domain, Amazon Craton: Constraints from SHRIMP and TIMS zircon, baddeleyite and titanite U–Pb geochronology. Precambrian Research 131, 73–109.

Silva, L.C., McNaughton, N.J., Melo, R.C., Fletcher, I.R., 1997. U–Pb SHRIMP ages in the Itabuna–Caríba TTG high-grade complex: the first window beyond the Paleoproterozoic overprinting of the eastern Jequié craton, NE Brazil. Proceedings 2nd International symposium on granites and associated mineralizations. Sociedade Brasileira de Geologia, Salvador-Bahia, pp. 282–283.

Silva, M.G., Coelho, C.E.S., Teixeira, J.B.G., Alves da Silva, F.C., Silva, R.A., Souza, J.A.B., 2001. The Rio Itapicuru greenstone belt, Bahia, Brazil: geologic evolution and review of gold mineralization. Mineralium Deposita 36, 345–357.

Silva, L.J.H.D., Dantas, E.L., Teixeira, J.B.G., Laux, J.H., Silva, M.G., 2007. U–Pb and Sm–Nd geochronology of amphibolites from the Curaçá Belt, São Francisco Craton, Brazil: Tectonic implications. Gondwana Research 12, 454–467.

Smith, B., Barley, M.E., Groves, D.I., Krapez, B., McNaughton, N.J., Bickle, M.J., Chapman, H.J., 1998. The Scholl Shear Zone, West Pilbara: evidence for a domain boundary structure from integrated tectonostratigraphic analyses, SHRIMP U–Pb dating and isotopic and geochemical data of granitoids. Precambrian Research 88, 143–171.

Souza, Z.S., 1984. Mapeamento geológico do "greenstone belt"do Rio Capim-BA — Área de Riacho das Pedras. Relatório de Graduação, Dept. Geologia, UFRN, 2 vols. 430 pp.

Souza, Z.S., 1986. Zonas de cisalhamento no greenstone belt do Rio Capim, NE da Bahia — Um modelo de deformação progressiva. XXXIV Congresso Brasileiro de Geologia, Sociedade Brasileira de Geologia, Goiânia, v. 2, pp. 678–694.

Souza, Z.S., Montel, J.M., Gioia, S.M.L.C., Hollanda, M.H.B.M., Nascimento, M.A.L., Sá, E.F.J., Amaro, V.E., Pimentel, M.M., Lardeaux, J.M., Veschambre, M., 2006. Electron microprobe dating of monazite from high-T shear zones in the São José de Campestre Massif, NE Brazil. Gondwana Research 9, 441–455.

Souza, Z.S., Martin, H., Peucat, J.J., Sá, E.F.J., Macedo, M.H.F., 2007. Calc-alkaline magmatism at the Archean–Proterozoic transition: the Caicó Complex Basement (NE Brazil). Journal of Petrology 48, 2149–2185.

Tamura, Y., Yuhara, M., Ishii, T., Irino, N., Shukumo, H., 2003. Andesites and dacites from Daisen Volcano Japan: partial-to-total remelting of an andesite magma body. Jounal of Petrology 44, 2243–2260.

Tassinari, C.C.G., Macambira, M., 1999. Geochronological provinces of the Amazonian Craton. Episodes 22, 174–182.

Teixeira, W., Figueiredo, M.C.H., 1991. An outline of Early Proterozoic crustal evolution in the São Francisco craton, Brazil: a review. Precambrian Research 53, 1–22.

Teixeira, W., Sabaté, P., Barbosa, J., Noce, C.M., Carneiro, M.A., 2000. Archean and Paleoproterozoic tectonic evolution of the São Francisco craton. In: Cordani, U.G., Milani, E.J., Thomaz Filho, A., Campos, D.A. (Eds.), Tectonic Evolution of South America. 31st International Geological Congress, Rio de Janeiro, pp. 101–137.

Teixeira, W., Geraldes, M.C., Matos, R., Ruiz, A.S., Saes, G., Vargas-Mattos, G., 2010. A review of the tectonic evolution of the Sunsás belt, SW Amazonian Craton. Journal of South American Earth Sciences 29, 47–60.

Vanderhaeghe, O., Ledru, P., Thiéblemont, D., Egal, E., Cocherie, A., Tegyey, M., Milési, J.P., 1998. Contrasting mechanism of crustal growth. Geodynamic evolution of the Paleoproterozoic granite–greenstone belts of French Guiana. Precambrian Research 92, 165–193.

Vendemiatto, M.A., Enzweiler, J., 2001. Routine control of accuracy in silicate rock analysis by X-ray fluorescence spectrometry. Geostandards Newsletter—The Journal of Geostandards and Geoanalysis 25, 283–291.

Winchester, J.A., Floyd, P.A., 1977. Geochemical discrimination of different magma series and their differentiation products using immobile elements. Chemical Geology 20, 325–343.

Winge, M., 1981. A Sequência Vulcano-sedimentar do Grupo Capim — Bahia: Caracterização geológica e modelo metalogenético. Master Dissertation, Departamento de Geociências, Universidade de Brasília, 120 pp.

Winge, M., Danni, J.C.M., 1980. Compartimentos geotectônicos prebrasilianos entre Caratacá e Bendengó, município de Uauá — Bahia. XXXI Congresso Brasileiro de Geologia, Sociedade Brasileira de Geologia, Camboriú, V. 5, pp. 2785–2795.

Woodhead, J.D., Eggins, S.M., Johnson, R.W., 1998. Magma genesis in the New Britain island arc: further insights into melting and mass transfer processes. Journal Petrology 39, 1641–1668.